Mycosphere

ARTICLE

Open Access

https://doi.org/10.48130/mycosphere-0026-0009

Mycosphere **2026**, 17: e009

Overexpression of Flfbp1 gene triggers the transition of *Fusarium lateritium* from a mutualistic endophyte to a pathogen via more β-Carboline production

Yongjie Li[1,2], Xingping Zha[2,3], Qing Xiao[1,2], Jiankang Wang[2,3], Guihua Liu[1,2], Rongfei Liu[1,2], Yongdong He[2,3], Zhangjiang He[2,3*] and Jichuan Kang[1,2*]

[1] *State Key Laboratory of Green Pesticide, Center for R & D of Fine Chemicals, Guizhou University, Guiyang 550025, China*
[2] *Engineering and Research Center for Southwest Biopharmaceutical Resource of National Education Ministry of China, Guizhou University, Guiyang 550025, China*
[3] *Department of Plant Pathology, College of Agriculture, Guizhou University, Guiyang 550025, China*
* Correspondence: zjhe3@gzu.edu.cn (He Z); jckang@gzu.edu.cn (Kang J)

Abstract

The transition from a symbiotic to a parasitic state is a widespread phenomenon among endophytes in nature. However, the underlying mechanisms regulating this transition remain largely unclear. Our study reveals that a conserved fungal virulence factor, the F-box protein Fbp1, and its homolog are involved in the transition from symbiosis to pathogenesis in the endophytic fungus *F. lateritium*. Knockout of *Flfbp1* in the endophytic *F. lateritium* significantly enhanced the colonization capacity of the strain in tobacco and improved its plant growth-promoting ability. Conversely, overexpression of *Flfbp1* led to a marked decrease in colonization rates and caused host plant lethality in tobacco. These results indicate that *Flfbp1* regulates the transition of the endophytic fungus from a symbiotic to a pathogenic state. Further mechanistic investigation demonstrated that Flfbp1 interacts with heat shock protein Flhsp1 to regulate the transcription of *Flsmp1*, a gene associated with β-Carboline synthesis, thereby mediating the synthesis of β-Carboline. This process disrupts auxin homeostasis in the plant, ultimately leading to plant death. This study identifies Flfbp1 as a core molecular switch that regulates the transition from symbiosis to pathogenesis in *F. lateritium* by modulating the synthesis of specific secondary metabolites.

Keywords: *Fusarium lateritium*, Flfbp1, β-Carboline, Symbiosis and pathogenicity, Auxin

Citation: Li Y, Zha X, Xiao Q, Wang J, Liu G, et al. 2026. Overexpression of Flfbp1 Gene Triggers the Transition of Fusarium lateritium from a Mutualistic Endophyte to a Pathogen via more β-Carboline production *Mycosphere* 17: e009 https://doi.org/10.48130/mycosphere-0026-0009

Introduction

Endophytes originated approximately 460 million years ago alongside the emergence of land plants, where they modulate diverse biological processes and sustain host fitness. During hundreds of millions of years of coevolution, endophytes have maintained evolutionarily independent strategies with remarkable lifestyle plasticity. They can dynamically shift between mutualistic and pathogenic states within the same host, governed by host–microbe genotypes, compatibility, and environmental cues; this plasticity underpins the stability and evolution of plant–microbe symbiotic systems[1,2]. Fungi, as the dominant group among endophytes, have been well documented for their lifestyle plasticity. Fungal groups such as endophytic, freshwater, and wood-rotting fungi in the special habitats of Southwest China exhibit high species diversity and habitat adaptability, enabling them to widely adapt to diverse hosts, substrates, and climates[3–7]. Unraveling the molecular regulatory mechanisms underlying such adaptation and lifestyle switching represents a core scientific question in the current research field. Current mechanistic understanding remains heavily skewed toward pathogenic fungi, for which regulatory frameworks are well-established. In contrast, the molecular basis underlying state transitions in endophytic fungi remains poorly defined—particularly in *Fusarium* species with dual symbiotic–pathogenic phenotypes. The identity of key regulators and core signaling pathways governing these switches remains elusive, constituting a critical knowledge gap in microbial symbiosis research.

In recent years, a series of breakthroughs have been made in understanding the molecular mechanisms governing lifestyle transitions in pathogenic fungi. Three core regulatory axes have been established, including transcriptional regulation, epigenetic modification, and secondary metabolite biosynthesis, providing a solid framework for dissecting analogous mechanisms in endophytic fungi[8–10]. Pioneering studies have identified several conserved and pivotal virulence regulators, such as the fungal F-box protein Fbp1, the *Pseudomonas syringae* effector HopF2, and the *Candida albicans* transcription factors Ume6/Efg1. Loss-of-function of these regulators directly triggers the switch between pathogenic and symbiotic lifestyles in pathogenic microbes[11–13]. Recent advances have further refined these regulatory networks. In *Magnaporthe oryzae*, MoSnt2 mediates epigenetic modification through histone deacetylation to precisely control the spatiotemporal expression of virulence genes, thereby enabling the transition between latent and pathogenic states[14]. In *Fusarium oxysporum*, the transcription factor FovSge1 determines fungal colonization ability and pathogenic phenotypes by modulating the effector secretome[15]. In *Verticillium dahliae*, VdPKS9 regulates the expression of secondary metabolite biosynthetic gene clusters to mediate microsclerotia formation and virulence[16]. In striking contrast, studies on endophytic fungi remain largely scarce. Several studies have identified key regulatory factors that control the transition between symbiotic and pathogenic states in certain fungi, for example, overexpression of the CtBOT6 transcription factor in *Colletotrichum tofieldiae* can directly convert this beneficial root endophyte into a pathogen[17]. However, such studies are limited to specific taxa and lack universal applicability. Most current investigations only describe fundamental phenotypes by adopting the framework

established for pathogenic fungi. Even in the widely studied genus *Fusarium*, only sporadic observations are available. *Fusarium foetens* produces the secondary metabolite FF-C1 to establish mutualistic symbiosis, and closely related strains can shift to a pathogenic lifestyle under environmental stress[18]. To date, the key regulators that govern the symbiotic–pathogenic transition in endophytic *Fusarium* remain unidentified.

Microbial secondary metabolites act as central mediators governing fungal lifestyle transitions and plant–fungus interactions, a concept that has been increasingly validated and expanded in recent investigations[19–22]. Among these metabolites, alkaloids represent pivotal effector molecules in cross-kingdom communication by virtue of their potent plant physiological regulatory activities, with β-Carboline as a paradigmatic example. Accumulating evidence has established that β-Carboline specifically inhibits polar auxin transport in plants by repressing the expression of PIN-family transporters, thereby markedly suppressing seedling growth in *Arabidopsis thaliana*. Notably, this inhibitory effect exhibits a clear concentration-dependent manner; elevated β-Carboline concentrations lead to progressively stronger inhibition and damage to root development and seed germination[23]. Nevertheless, β-Carboline compounds identified to date are exclusively isolated from plants and bacteria. Whether members of the genus *Fusarium* are capable of synthesizing β-Carboline remains unknown, and the precise molecular pathways by which β-Carboline mediates endophytic fungus–plant interactions remain largely elusive. Meanwhile, auxin homeostasis constitutes a core regulatory module for plant growth and development, as well as a critical hub for establishing microbe–plant symbiosis[24,25]. Auxin transport represents a central step in the precise spatiotemporal control of auxin signaling, and its disruption directly impairs normal plant development and disturbs symbiotic relationships within the microbial niche[26,27]. However, current studies have predominantly focused on the regulation of auxin transport by plant-encoded genes. The mechanism by which endophytic fungi modulate host auxin transport via endogenous metabolites to orchestrate their own symbiotic–pathogenic switch remains largely unexplored. This represents a critical knowledge gap in dissecting the molecular basis underlying endophytic fungus–plant interactions.

In this study, we characterize an endophytic strain *F. lateritium* Fl617 that confers plant growth promotion and disease resistance in several Solanaceae species[28–31]. Transcriptomic profiling of the *F. lateritium* Fl617–plant interaction revealed that a gene encoding an F-box protein, designated Flfbp1, was significantly down-regulated during host colonization. This expression pattern is in sharp contrast to that of the homologous Fbp1 characterized in pathogenic fungi, implying divergent functional roles of F-box proteins between endophytic and pathogenic lifestyles. Further analyses demonstrated that Flfbp1 mediates the reversible switch of *F. lateritium* Fl617 between symbiotic and pathogenic states, independent of fungal colonization levels. Importantly, β-Carboline, a secondary metabolite under the direct control of Flfbp1, acts as the key effector governing this lifestyle transition. Transcriptional activation of the β-Carboline biosynthetic gene cluster promotes metabolite accumulation and triggers pathogenicity in planta. Conversely, genetic disruption of the biosynthetic gene reduces β-Carboline production and shifts the fungus toward a plant growth-promoting endophytic phenotype. Moreover, we demonstrate that β-Carboline modulates plant growth by suppressing auxin transport. Collectively, this study identifies the master regulator Flfbp1 that governs the symbiotic–pathogenic switch in endophytic *F. lateritium* Fl617, and provides the first evidence that members of the genus *Fusarium* can synthesize β-Carboline. We further delineate the molecular mechanism by which β-Carboline orchestrates fungus–plant cross-kingdom communication. These findings not only offer novel insights into the molecular regulatory basis underlying lifestyle transitions in endophytic fungi but also establish a new paradigm for understanding how microbial secondary metabolites shape the dynamic interplay between fungi and their host plants.

Material and methods

Fungal and plant growth conditions

Wild-type and mutant strains of *F. lateritium* were cultured on PDA at 28 °C, while *N. benthamiana* seedlings were grown in a Walk-in Chamber (WIPGC-BP83.Fujian Jiupo Biotechnology Co., Ltd) at 25 °C under a 16 h light/8 h dark photoperiod.

In this study, *N. benthamiana* was selected as the host plant for three major reasons. First, the fungal strain confers plant growth promotion and disease resistance in Solanaceae species, and *N. benthamiana* is ideal for molecular mechanism studies under laboratory conditions. Second, as a well-established model plant, *N. benthamiana* possesses a well-annotated genome and is highly amenable to molecular manipulations. Third, its short life cycle and easily observable and quantifiable phenotypes greatly improve experimental efficiency.

Co-cultivation experiment of *F. lateritium* and *N. benthamiana*

N. benthamiana seed pretreatment: Seeds were rinsed five times with sterile water to remove shrivelled, dry, and insect-damaged ones. They were then soaked in 2% NaClO for 10 min, followed by five rinses with sterile water to eliminate residual NaClO. The seeds were placed in Petri dishes lined with moist filter paper and incubated at 25 °C under a 16 h light/8 h dark photoperiod for 1 week. After the seeds germinate, the seedlings are transplanted into a fresh MS medium containing 3% sucrose and continue to be cultured for 3 weeks.

Preparation of *F. lateritium* spore suspension: Six mycelial plugs (0.5 cm in diameter) were taken from the edge of the mycelium using a punch and inoculated into 50 ml of 1/4 SDB medium. The culture was incubated at 150 rpm for 3–5 d. The spore suspension was collected by filtering the mycelium through three layers of filter paper, and the final concentration was adjusted to 5×10^5 spores/mL.

Co-cultivation operation: inoculate 5 μL spore suspension 2 cm below the tobacco root and co-culture at 25 °C under a 16 h light/8 h dark photoperiod. Each treatment and control group consisted of 30 tobacco seedlings co-cultivated with the fungal strain.

Confocal microscopy

The roots of axenic seedlings of *N. benthamiana* were immersed in a spore suspension of *F. lateritium* (5×10^5 conidia/mL) for 10 min for inoculation. After co-cultivation for 3, 5, 7, and 10 d, respectively, roots were harvested and cut into 1 cm-long segments. Root segments were then treated with a 10% KOH solution in a boiling water bath for 6 min, and rinsed twice with sterile water to remove residual KOH. The cleared root segments were placed in a mixed staining solution containing WGA488 (10 μg/mL) and PI (15 μg/mL), and incubated in the dark for 30 min for staining. After staining, segments were rinsed one to two times with phosphate-buffered saline (PBS, pH 7.4) to remove unbound free dyes on the surface and

reduce background fluorescence interference. The treated samples were then mounted on a glass slide with 20% glycerol and observed using a LSM900 confocal laser scanning microscope. WGA488 (AF 488) is excited with a 488 nm argon laser, and the emitted light is collected via a hybrid detector in the 500–550 nm wavelength range; PI is excited with a 532 nm argon ion laser, and the emitted light is collected via a hybrid detector in the 600–660 nm wavelength range[32].

Observation of fungal colonization patterns

Roots of *N. benthamiana* were inoculated with fungal spore suspensions (WT, Δ*Flfbp1*, *Flfbp1*^{OE}, and Δ*Flfbp1-C*) at a concentration of 5×10^5 spores/mL.The spore suspension was prepared as follows: strains were cultured in 1/4 SDB medium at 28 °C for 7 d. Spores were harvested, washed with sterile water, filtered to remove mycelia, and the concentration was adjusted to 5×10^5 spores/mL. After inoculation, plants were incubated at 28 °C under a 16 h light/8 h dark photoperiod with 60% relative humidity for 7 d. After incubation, tobacco root tissues were collected and gently washed three times with a sterile PBS buffer to remove residual non-invaded fungi on the surface. Roots were then fixed in 50% FAA fixative at 4 °C for 24 h, followed by paraffin embedding and sectioning performed by Servicebio (Wuhan, China; www.servicebio.cn). Paraffin sections were dewaxed and rehydrated sequentially in: dewaxing transparent solution I (room temperature, 20 min), dewaxing transparent solution II (room temperature, 20 min), anhydrous ethanol I (5 min), anhydrous ethanol II (5 min), and 75% ethanol (5 min), followed by rinsing with tap water 3 times for 2 min each. Sections were placed in a dark, humid chamber and stained with a mixture containing 10 μg/mL fluorescein-labeled wheat germ agglutinin (WGA488) and 15 μg/mL propidium iodide (PI) in the dark at room temperature for 30 min. After staining, an LSM900 laser scanning confocal microscope (Zeiss) was used for observation. WGA488 was excited by a 488 nm argon laser, and emission was collected at 500–550 nm (labeling plant cell walls/membranes, green signal). PI was excited by a 532 nm laser, and emission was collected at 600–660 nm (labeling nuclei, red signal)[32].

RNA extraction and reverse transcription-quantitative polymerase chain reaction (RT-qPCR)

Total RNA was extracted using the Rapid RNA Extraction Kit (RNApure Plant Kit from CWbio) according to the manufacturer's instructions. First-strand cDNA synthesis was performed using the StarScript II First-Strand cDNA Synthesis Kit. Quantitative PCR was carried out with SYBR Green qPCR Mix (Monad) on a Bio-Rad detection system. The $2^{-\Delta Ct}$ method was used to calculate changes in gene expression[33], with *NbEFLA* serving as the endogenous control.

Colonization rate determination

The fungus/plant DNA ratio (FPDR) was used to monitor fungal infection in *N. benthamiana* roots[34]. FPDR plays an important role in eliminating errors caused by differences in fungal inoculum amounts. Additionally, FPDR allows for the assessment of whether endophytic fungal colonization affects *N. benthamiana* root growth and whether *N. benthamiana* root growth influences endophytic fungal infection. The degree of fungal infection was determined using the $2^{-\Delta Ct}$ method, where ΔCt represents the difference between the threshold cycle (Ct) values of the *F. lateritium Flfbp1* gene and the *N. benthamiana* EF-1α gene. Genomic DNA was extracted from *N. benthamiana* roots following interaction with the strains (which includes the *F. lateritium* genome) for quantitative real-time PCR analysis.

Root calcofluor white (CFW) staining in the fungus-tobacco co-culture system

Intact root samples were collected from tobacco co-cultured with different *F. lateritium* strains, and gently rinsed three times with sterile water to remove free hyphae on the surface and residual medium. The roots were evenly spread on a clean glass slide, and an appropriate amount of CFW staining solution was added to fully immerse the root tissue. After covering with a coverslip, the samples were incubated in the dark at room temperature for 5 min. The coverslip was carefully removed, and the root surface was gently rinsed 4–5 times with washing buffer to thoroughly remove unbound dye and reduce background fluorescence. Excess liquid was absorbed along the edge of the slide with absorbent paper. Fluorescence images were captured under a laser scanning confocal microscope using an excitation wavelength of 355 nm and an emission wavelength of 440 nm. Specific bright blue fluorescent signals from tobacco root cell walls and colonized hyphae were observed[35].

Construction of the *Flfbp1*, *Flhsp1* and *Flsmp1* knockout, overexpression, and complementation mutants in *F. lateritium* Fl617

Construction of the *Flfbp1*, *Flhsp1*, and *Flsmp1* knockout mutants: to construct knockout mutants of *Flfbp1*, *Flhsp1*, and *Flsmp1* in *F. lateritium*, the Fl617 strain was used as the recipient. The upstream and downstream homologous arms of each gene and the hygromycin resistance selection marker were amplified by overlap PCR, and the gene knockout fusion fragments were constructed by fragment ligation. The knockout fusion fragments were introduced into *F. lateritium* protoplasts via PEG-mediated fungal protoplast transformation, and the transformed products were spread on TB3 solid medium containing 25 μg/mL hygromycin, followed by incubation at 28 °C until single colonies appeared for primary screening[36]. Single colonies of primary positive transformants were picked and purified for culture, and the genomic DNA of the purified strains was rapidly extracted by the alkaline lysis method. Gene-specific verification primers were designed for PCR amplification and identification to obtain homozygous gene knockout mutants. The bacterial suspension of positive mutants was mixed with 25% glycerol at an equal volume and stored at −80 °C for later use.

Construction of *Flfbp1* overexpression mutants: *Flfbp1* overexpression transformants were generated via *Agrobacterium tumefaciens* (AGL1)-mediated genetic transformation[37]. A single colony of *A. tumefaciens* harboring the plasmid vector (pK2-hyg-gpdA::*Flfbp1*) was inoculated into YCK liquid medium (supplemented with 50 μg/mL kanamycin [Kana] and 50 μg/mL carbenicillin [Car]) and cultured overnight (24 h) at 28 °C with shaking at 200 rpm. Bacterial cells were collected by centrifugation at 6,000 rpm for 10 min at 4 °C, resuspended in an appropriate volume of IM liquid medium (containing 400 μmol/L acetosyringone and 10 mmol/L glucose), and the concentration of the resuspended bacterial solution was adjusted to an OD_{600} of 0.15, followed by incubation at 28 °C with shaking at 180 rpm for approximately 6 h. Meanwhile, fresh *Fusarium* blastospores (cultured in 1/4 SDB medium at 28 °C with shaking at 180 rpm for 5 d) were dispersed in IM liquid medium, filtered through sterile lens paper to remove mycelia, and after thorough vortexing, the spore concentration was adjusted to a suitable level.

An equal volume of the spore suspension and *Agrobacterium* suspension was mixed, and 100 μL of the mixture was spread onto a microporous filter membrane placed on IM solid medium plates (containing 200 μmol/L acetosyringone and 5 mmol/L glucose), followed by co-cultivation at 22 °C for 48 h. The co-cultured filter membrane was transferred to CZM medium (containing 1 mg/mL cephalosporin and 25 μg/mL hygromycin) for screening. DNA was rapidly extracted using the alkaline lysis method, followed by PCR detection. Correct *Flfbp1*^{OE} mutants were obtained and stored in 25% glycerol.

Construction of gene complementation mutants: using the identified homozygous knockout mutants of *Flfbp1*, *Flhsp1*, and *Flsmp1* as recipient strains, the corresponding gene complementation mutants were constructed via PEG-mediated protoplast transformation. Using the genomic DNA of WT strain Fl617 as the template, the complete open reading frame of each target gene was amplified by PCR, and its own 1.5–2.0 kb promoter region sequence was ligated simultaneously. The amplified fragment was ligated into a fungal expression vector to construct a recombinant complementation vector, which was linearized for later use after being verified correct by double enzyme digestion and sequencing. Protoplasts of the recipient strains were prepared with reference to the above method, and the linearized recombinant complementation vector was introduced into the protoplasts, followed by spreading on TB3 medium containing 10 μg/mL G418 and incubation at 28 °C in the dark until single colonies appeared. Single colonies were picked and purified for culture, and genomic DNA was extracted and identified by PCR with target gene-specific primers to obtain the correct complementation mutants, which were stored in 25% glycerol for later use.

Construction of *Flhsp1* knockout mutants in *Flfbp1*^{OE} strain: to construct knockout mutants of *Flhsp1* in *F. lateritium*, the *Flfbp1*^{OE} strain was used as the recipient. The upstream and downstream homologous arms of each gene and the G418 resistance selection marker were amplified by overlap PCR, and the gene knockout fusion fragments were constructed by fragment ligation. The knockout fusion fragments were introduced into *F. lateritium* protoplasts via PEG-mediated fungal protoplast transformation, and the transformed products were spread on TB3 solid medium containing 10 μg/mL hygromycin, followed by incubation at 28 °C until single colonies appeared for primary screening. Single colonies of primary positive transformants were picked and purified for culture, and the genomic DNA of the purified strains was rapidly extracted by the alkaline lysis method. Gene-specific verification primers were designed for PCR amplification and identification to obtain homozygous gene knockout mutants. The bacterial suspension of positive mutants was mixed with 25% glycerol at an equal volume and stored at −80 °C for later use.

Determination of cysteine protease activity in roots

N. benthamiana roots were inoculated with WT, Δ*Flfbp1*, and *Flfbp1*^{OE} strains, respectively. Plant samples were harvested 10 d post-inoculation and frozen in liquid nitrogen. A 0.1 g aliquot of ground roots was extracted with a buffer containing 100 mM sodium acetate (pH 5.5), 100 mM sodium chloride, 1 mM ethylenediaminetetraacetic acid (EDTA), 2 mM dithiothreitol (DTT), and 1 mM phenylmethylsulfonyl fluoride. To determine cysteine protease activity, 100 μM fluorescent VPE substrate (Ac-ESEN-MCA, Peptide Institute) was added to the root extract, and fluorescence intensity at 465 nm was measured using a fluorescent microplate reader with excitation at 360 nm[38].

Co-cultivation of *F. lateritium* and *N. benthamiana* seedlings with β-Carboline treatment

Three-week-old axenic seedlings of *N. benthamiana* and a single-spore strain of *F. lateritium* (spore concentration: 5×10^5 spores/mL) were used. A β-Carboline solution of a specific concentration was prepared and added to the MS medium; an ethanol solvent control and a blank control were also set up. Tobacco seedlings were transplanted in the center of MS plates, and 5 μL of the spore suspension was inoculated 5 cm below the seedling roots. The plates were placed in an incubator at 25 °C for co-cultivation under a 16 h light/8 h dark photoperiod[39].

Yeast two-hybrid (Y2H) assay

To investigate the interaction between Flfbp1 and Flhsp1, the coding sequence of *Flfbp1* was cloned into pGBKT7 (BD) to construct the recombinant vector BD-*Flfbp1*, and the coding sequence of *Flhsp1* was cloned into pGADT7 (AD) to construct the recombinant vector AD-*Flhsp1*. These vectors were co-transformed into the yeast strain Y2HGold. Positive clones were screened on SD-Trp-Leu (SD-TL) agar containing X-α-Gal and further confirmed on SD-Trp-Leu-His-Ade (SD-TLHA) agar (Coolaber) containing X-α-Gal. NC (negative control): Y2HGold strain transformed with pGBKT-Lam + pGADT7-T. PC (positive control): Y2HGold strain transformed with pGBKT-53 + pGADT7-T[40].

Bimolecular fluorescence complementation (BiFC) assay

The coding sequences of *Flfbp1* and *Flhsp1* were cloned into the bimolecular fluorescence complementation vectors pCV-nYFP and pCV-cYFP, respectively. *Agrobacterium* strains harboring the recombinant vectors Flfbp1-nYFP and Flhsp1-cYFP were co-infiltrated into *N. benthamiana* leaves. After 2 d, YFP fluorescence signals in the infiltrated areas were detected using an LSM900 laser scanning confocal microscope[40].

Co-immunoprecipitation (Co-IP) assay

The coding sequences of Flfbp1 and Flhsp1 were cloned into pCAMBIA1300-mCherry and pCAMBIA1300-GFP vectors, respectively. Flfbp1-mCherry and Flhsp1-GFP were co-expressed in *N. benthamiana* leaves via injection. Proteins were extracted using a protein extraction buffer containing 0.1% (v/v) protease inhibitor and 0.1% (v/v) PMSF. Anti-GFP magnetic beads were used for Co-IP detection according to the manufacturer's manual. Briefly, 20 μL of magnetic beads were co-incubated with 500 μL of protein sample with gentle shaking at 4 °C for 3 h. After incubation, the beads were washed five times with protein extraction buffer. The eluted proteins were boiled for 10 min in a solution containing 40 μL PBS and 10 μL SDS-PAGE loading buffer, separated by SDS-PAGE, and analyzed using anti-GFP or anti-mCherry antibodies[41].

Flhsp1 protein site-directed mutagenesis experiment

Potential ubiquitination sites of the Flhsp1 protein were analyzed using the website https://gpsuber.biocuckoo.cn/userguide.php. Primers were designed to mutate the conserved lysine (K) residue at position 8 of this protein to arginine (R), and site-directed mutagenesis was performed via PCR[42]. The sequences of the primers used are as follows:

Primer F: gaacacgggggacgagctcATGAGTGACAACGCTGGTTCAAG GGCGGGC;

Primer R: tgtcgactctagaggatccGATGTTTCCTCGTACACCAC.

Metabolite extraction and quantification

A 0.1 g aliquot of crude extract from samples of plant interaction with *F. lateritium* strains was collected, freeze-dried, ground into a fine powder in liquid nitrogen, and then dissolved in methanol. The mixture was sonicated for 30 min, filtered through a 0.25 μm microporous membrane, and stored at 4 °C. For homogenized samples, β-Carboline (1 mg/mL) was added as an internal standard. After filtration through a 0.25 μm microporous membrane, the samples were stored at 4 °C for HPLC analysis. Metabolites were analyzed using a high-performance liquid chromatography (HPLC, Agilent 1290) system equipped with an Agilent Poroshell 120 SB-C18 column (100 × 2.1 mm, 2.7 μm). For β-Carboline analysis, the mobile phase consisted of 60% methanol/50 mM ammonium acetate (pH 8). Samples were eluted at a flow rate of 0.8 mL/min for 15 min. A series of concentrations of each standard compound was prepared and analyzed in parallel with the samples to generate standard curves for metabolite quantification[43]. Each test sample was set up with three biological replicates for detection.

Determination of abiotic stress tolerance and conidiation in *F. lateritium* strains

Fresh blastospores were collected from each strain cultured in 1/4 SDB liquid medium for 5 d. Spore suspensions were prepared with 0.05% (v/v) Tween-80, counted using a hemocytometer, and adjusted to a concentration of 5×10^5 conidia/mL for subsequent assays of abiotic stress tolerance and conidiation. For abiotic stress tolerance analysis, 3 μL of the spore suspension (5×10^5 conidia/mL) was spot-inoculated onto basal media including PDA, MS, and MM (as untreated control), as well as MM media supplemented with 0.8 M NaCl, 5.76 mM H_2O_2, 25 μg/mL Congo Red, or adjusted to pH 5.4 or pH 10.4. All plates were incubated at 28 °C for 7 d under light or dark conditions. Colony morphology was photographed, and colony growth rate was measured using the cross-crossing method. For conidiation assays, 100 μL of the spore suspension (5×10^5 conidia/mL) was inoculated into 1/4-strength SDB medium and incubated at 28 °C with shaking at 180 rpm under light for 7 d before quantification. Each treatment was performed with three independent replicates, and all experiments were repeated three times.

Histochemical Gus staining of roots in the fungus–*Arabidopsis thaliana* co-culture system

Intact root samples were harvested from *Arabidopsis thaliana* co-cultivated with different *F. lateritium* strains and gently rinsed three times with sterile water to thoroughly remove free hyphae and residual medium from the root surface. Roots were placed without overlapping into centrifuge tubes and fully immersed in GUS staining solution. Samples were incubated in the dark at 37 °C overnight in a constant-temperature incubator. Once distinct blue coloration appeared at the target sites, the staining solution was discarded, and roots were destained 2–3 times in 70% ethanol until the negative control tissues became colorless. The destained roots were rinsed once with sterile water, gently spread on a clean glass slide with a small volume of sterile water, and observed under a stereomicroscope[44].

RNA extraction and RNA-sequencing analyses

Roots of *F. lateritium* or *N. benthamiana* seedlings at the specified co-culture time were selected as samples for transcriptome detection. To ensure data reliability, three biological replicates were set for each group (each replicate contained 30 *N. benthamiana* seedlings for the tobacco group and 30 culture plates of *F. lateritium* for the fungal strain group). Immediately after collection, the samples were rapidly frozen in liquid nitrogen, then transferred to −80 °C for low-temperature storage to prevent RNA degradation, and subsequently sent to Majorbio Bio-pharm Technology Co., Ltd. for follow-up experiments. In the experiment, total RNA was extracted using TRIZOL reagent, and multiple quality control steps were conducted after extraction to ensure quality: the purity standard was $OD_{260/280}$ ≈1.8–2.2, a spectrophotometer was used to detect RNA concentration and purity, while RNA integrity was verified by denaturing agarose gel electrophoresis, and sequencing was carried out only after confirming the samples fully met the experimental requirements. For the sequencing stage, the Illumina Novaseq 6000 or HiSeq 3000 platform was selected. During data analysis, Trimmomatic software was first used to remove low-quality reads and adapter sequences, followed by alignment and quantification of the processed data; then, the R packages tximport and DESeq2 were used to calculate the log2 fold change in gene expression and conduct differential expression analysis. Finally, differentially expressed genes were screened with the threshold of FDR-adjusted p-value < 0.05, functional enrichment analysis of differentially expressed genes was performed using Blast2GO software (www.blast2go.com/b2ghome), while KEGG metabolic pathway analysis was conducted with Cytoscape software (www.cytoscape.org/) and its plugin ClueGO (www.ici.upmc.fr/cluego/cluegoDownload.shtml). KEGG pathway analyses were performed using the KEGG database[45], with all experimental data deposited in the NCBI GEO database for archiving[32].

Statistical analyses

For the statistical analysis of relative gene expression levels, the group with the highest data stability and reproducibility was first selected from three candidate groups, and the final relative gene expression level was determined as the mean value of three biological replicates within this optimal group, ensuring data reliability and statistical power.

All quantitative data are presented as the mean ± standard deviation (SD) of at least three independent biological replicates. For comparisons between two groups, statistical significance was determined using an unpaired Student's t-test. For experiments involving three or more groups, one-way analysis of variance (ANOVA) was performed, followed by Tukey's Honestly Significant Difference (HSD) post hoc test to identify specific inter-group differences.

Results

Identification of core candidate genes mediating the interaction of endophytic *F. lateritium* Fl617 with diverse hosts and functional characterization of Flfbp1

Host specificity represents a prominent and conserved feature in endophytic fungus–plant interactions. Unraveling the molecular regulatory mechanisms governing such specificity remains a central scientific challenge in the field of microbe–plant communications. Our previous work demonstrated that the endophytic strain *F. lateritium* Fl617 exhibits distinct and stable phenotypic divergence when interacting with hosts from different plant families. Specifically, this strain establishes a typical mutualistic symbiosis with solanaceous plants, including tobacco, tomato, and potato, significantly promoting host growth and enhancing disease

resistance[28–31]. In contrast, when interacting with sorghum (Poaceae) and oilseed rape (Brassicaceae), Fl617 shows no obvious growth-promoting effects, but also does not inhibit host development or cause disease symptoms, maintaining a stable commensal interaction (unpublished data). Such differential interaction patterns across distantly related host plants strongly suggest the existence of core regulators in Fl617 that govern host-specific symbiotic adaptation, whose expression profiles are likely tightly linked to fungal perception and accommodation of distinct host environments. To identify these key regulators, we systematically analyzed transcriptomic data of *F. lateritium* Fl617 during root colonization of three representative hosts: tomato, sorghum, and oilseed rape. We focused on genes displaying consistent expression changes across all three hosts, as this strategy effectively excludes non-specific responses induced by host-specific signals and enriches for fungal-intrinsic core regulators of symbiosis. Conserved expression patterns of these genes are proposed to serve as a critical molecular basis for the stable establishment of interactions between Fl617 and diverse host plants. The present study aimed to identify key conserved candidate genes involved in the broad-host interaction of *F. lateritium* Fl617, thereby laying a foundation for dissecting the molecular mechanisms by which these core genes control fungal symbiotic lifestyles.

Based on this screening strategy, in-depth transcriptomic analysis revealed that a gene annotated as encoding an F-box-like protein was significantly downregulated in Fl617 during interactions with all three distantly related plant species (Supplementary Fig. S1). This conserved down-regulation pattern across hosts implies that this gene may act as a core candidate regulator of fungal–host interactions. Further analysis showed that the gene encodes a 529-amino-acid protein, sharing 98%, 88%, and 87% identity with orthologs from *F. solani*, *F. oxysporum*, and *F. pseudograminearum*, respectively. The protein contains an F-box domain at residues 125–164 aa and six WD40 domains at residues 190–529 (Fig. 1a, b). Three-dimensional structural modeling using SWISS-MODEL predicted a typical F-box protein architecture (Fig. 1c), with a conserved Protein-Ligand Interaction Site (PLIP) including six conserved residues: G350, L354, A369, R375, W377, and R384. This structure is highly similar (95% identity) to the SCF^{Cdc4} ubiquitin ligase complex[46]. Accordingly, the protein was designated FlFbp1 (*F. lateritium* F-box Protein 1). BLAST homology searches using the FlFbp1 sequence indicated that this protein is unique and highly conserved within the genus *Fusarium* (Fig. 1d). Previous studies reported that the conserved virulence-associated F-box protein Fbp1 is transcriptionally activated in fusaria such as *F. oxysporum* and *F. graminearum*[11,4748]. In striking contrast, *Flfbp1* in the endophytic *F. lateritium* Fl617 was significantly repressed upon root interaction with host plants. We therefore hypothesize that FlFbp1 functions as a key regulator that modulates the symbiotic lifestyle of endophytic *F. lateritium* Fl617 and participates in the regulation of fungus–plant interactions.

In *N. benthamiana*, Flfbp1 orchestrates the transition of endophytic *F. lateritium* from a symbiotic to a pathogenic lifestyle

To investigate the role of Flfbp1 in endophytic *F. lateritium* during fungus–plant interactions, we initially selected *N. benthamiana* as the host and profiled *Flfbp1* expression dynamics. *Flfbp1* was found to be significantly downregulated throughout the entire interaction period (Supplementary Fig. S2a–S2d), consistent with its expression patterns in sorghum, rapeseed, and tomato. This conserved expression across diverse hosts excludes host-specific effects on Flfbp1 function, supporting the use of *N. benthamiana* as a model for subsequent functional assays. We further generated the *Flfbp1* knockout mutant (Δ*Flfbp1*), overexpression mutant (*Flfbp1*^{OE}), and complemented strain (Δ*Flfbp1-C*) using targeted gene knockout and ectopic overexpression techniques (Supplementary Fig. S3), and these mutants were inoculated into *N. benthamiana* under axenic conditions on MS medium to evaluate phenotypic outcomes. Continuous observation at 3, 5, 7, and 10 d after inoculation showed that *N. benthamiana* inoculated with the WT strain exhibited obvious growth promotion, with significantly higher biomass than the CK (Supplementary Fig. S4). In contrast, *N. benthamiana* inoculated with *Flfbp1*^{OE} displayed progressive wilting and eventual death (Fig. 2a–d), and its biomass was significantly lower than that of the WT-treated group (Fig. 2e). Plants inoculated with Δ*Flfbp1* showed remarkably enhanced growth promotion (Fig. 2a–d) and significantly increased biomass (Fig. 2e). Inoculation with the complemented strain Δ*Flfbp1-C* restored growth promotion to a level similar to that of the WT group, with no significant difference in biomass (Fig. 2a–e). Vacuolar processing enzymes (VPEs) are key regulators of plant programmed cell death (PCD). VPE activity assays revealed that VPE activity in *N. benthamiana* inoculated with *Flfbp1*^{OE} was 1.2-fold higher than that in the WT group ($p < 0.01$). VPE activity in the Δ*Flfbp1*-treated group decreased significantly to 87.7% of the WT level ($p < 0.01$), whereas no significant difference was observed between the Δ*Flfbp1-C* complemented strain and the WT group (Supplementary Fig. S2e).

The fungal colonization assay revealed that disruption of the Flfbp1 gene significantly increased the colonization amount of the strain in plants, and the colonization amount further increased significantly with the extension of the interaction time. On the contrary, the colonization rate of the Flfbp1 overexpression strain decreased significantly. The colonization level of the Δ*Flfbp1-C* complemented strain was comparable to that of the WT strain (Fig. 2f). In addition, regarding the fungal colonization pattern, root cross-sections are also crucial for examining the colonization intensity and sites of the fungus. Observations of tobacco root cross-sections inoculated with the WT, Δ*Flfbp1*, *Flfbp1*^{OE}, and Δ*Flfbp1-C* strains revealed no significant differences in root tissue structure among the groups (Supplementary Fig. S5). Fungal hyphae were consistently distributed in the cortical cells, indicating that the colonization sites were not altered by genotype. Significant differences were observed in fungal colonization intensity; roots inoculated with the WT, Δ*Flfbp1*, and Δ*Flfbp1-C* strains showed strong colonization signals, while the signal intensity was significantly reduced in roots inoculated with the *Flfbp1*^{OE} strain (Supplementary Fig. S5). These results indicate that plant cell necrosis induced by *Flfbp1*^{OE} was not caused by excessive fungal proliferation, thus excluding a colonization-dependent pathogenic pattern. Combining the above experimental results, our findings suggest that Flfbp1 acts as a key regulator that controls the transition of the interaction between *F. lateritium* Fl617 and *N. benthamiana* from a symbiotic to a pathogenic lifestyle.

To further verify the conserved function of Flfbp1 in mediating the switch between symbiotic and pathogenic states of *F. lateritium* Fl617 across diverse hosts, we performed cross-host inoculation assays using the model plant *Arabidopsis thaliana* and the Solanaceous crop *Solanum lycopersicum*. Plants were co-cultured with fungal strains for 10 d. The results showed that *Arabidopsis thaliana* inoculated with the WT strain exhibited significant growth promotion, with 4.82-fold higher biomass than the uninoculated control (CK) ($p < 0.01$). *Arabidopsis thaliana* inoculated with the Δ*Flfbp1* strain showed even stronger growth promotion, with 1.89-fold higher biomass than the WT-treated group ($p < 0.01$). In contrast, *Arabidopsis* inoculated with the *Flfbp1*^{OE} strain displayed a lethal

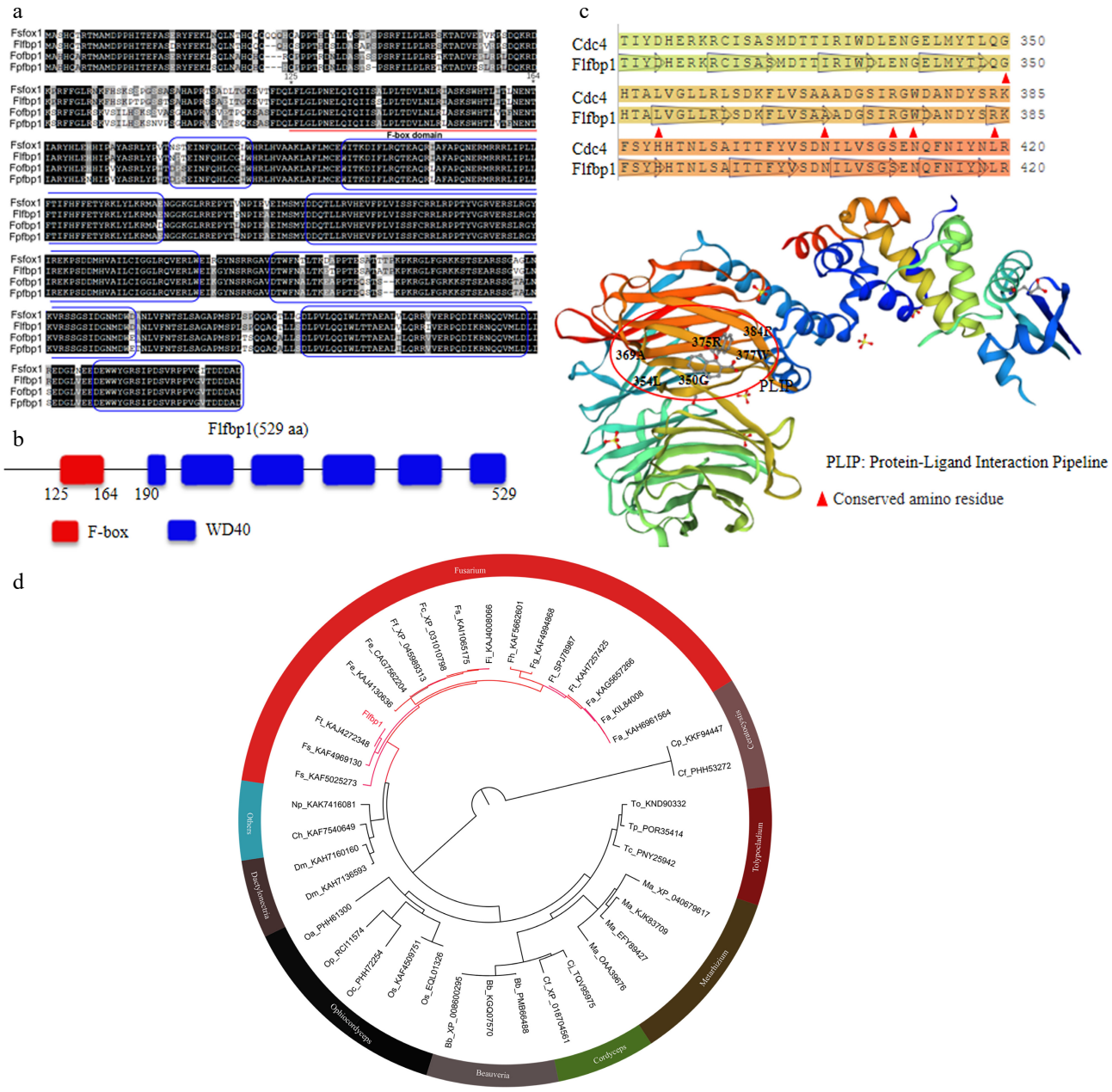

Fig. 1 Prediction of Flfbp1 protein domains. (a) Homologous alignment and domain prediction of the *Flfbp1* gene. Using the Flfbp1 protein as a probe, blast alignment was performed on its homologous protein sequences to predict conserved domains. The F-box domain is marked with a red underline, and the WD40 domain is marked with a blue box. (b) Schematic diagram of the Flfbp1 protein structure. (c) Prediction of the three-dimensional structure and conserved amino acid sites of Flfbp1. The three-dimensional structure was modeled using SWISS-MODEL with the Flfbp1 protein as a probe; red triangles mark conserved amino acid residues, and red circles indicate protein-ligand interaction regions (PLIP) composed of conserved residues. (d) Retrieval of homologous genes of this protein using the Flfbp1 protein sequence as a probe.

phenotype, similar to that observed in tobacco (Supplementary Fig. S6a, S6b). In the tomato inoculation system, both WT and Δ*Flfbp1* strains significantly promoted host growth and biomass accumulation, and the growth-promoting effect of Δ*Flfbp1* was significantly stronger than that of the WT, which was highly consistent with the phenotypes observed in *Arabidopsis thaliana* and *N. benthamiana*. However, inoculation with the *Flfbp1*^{OE} strain only caused severe growth inhibition in tomato plants, without a lethal phenotype (Supplementary Fig. S6a, S6c). Together, these cross-host validation results demonstrate that *Flfbp1* acts as a core molecular switch controlling the symbiosis–pathogenicity transition of *F. lateritium* Fl617, and its regulatory function is conserved across plant species. In contrast, the intensity of Flfbp1-mediated pathogenicity is modulated by the host genetic background.

Flfbp1 regulates the biosynthesis of cell wall-degrading enzymes and fungal secondary metabolites

To explore the molecular mechanism by which the *Flfbp1*^{OE} strain induces tobacco death, transcriptome analysis of fungus–plant interactions revealed that overexpression of *Flfbp1* regulated the differential expression of 155 genes in *F. lateritium*. Among them, 130 were upregulated, and 25 were downregulated (Supplementary Fig. S7a, S7b). GO and KEGG functional enrichment analyses of

https://doi.org/10.48130/mycosphere-0026-0009

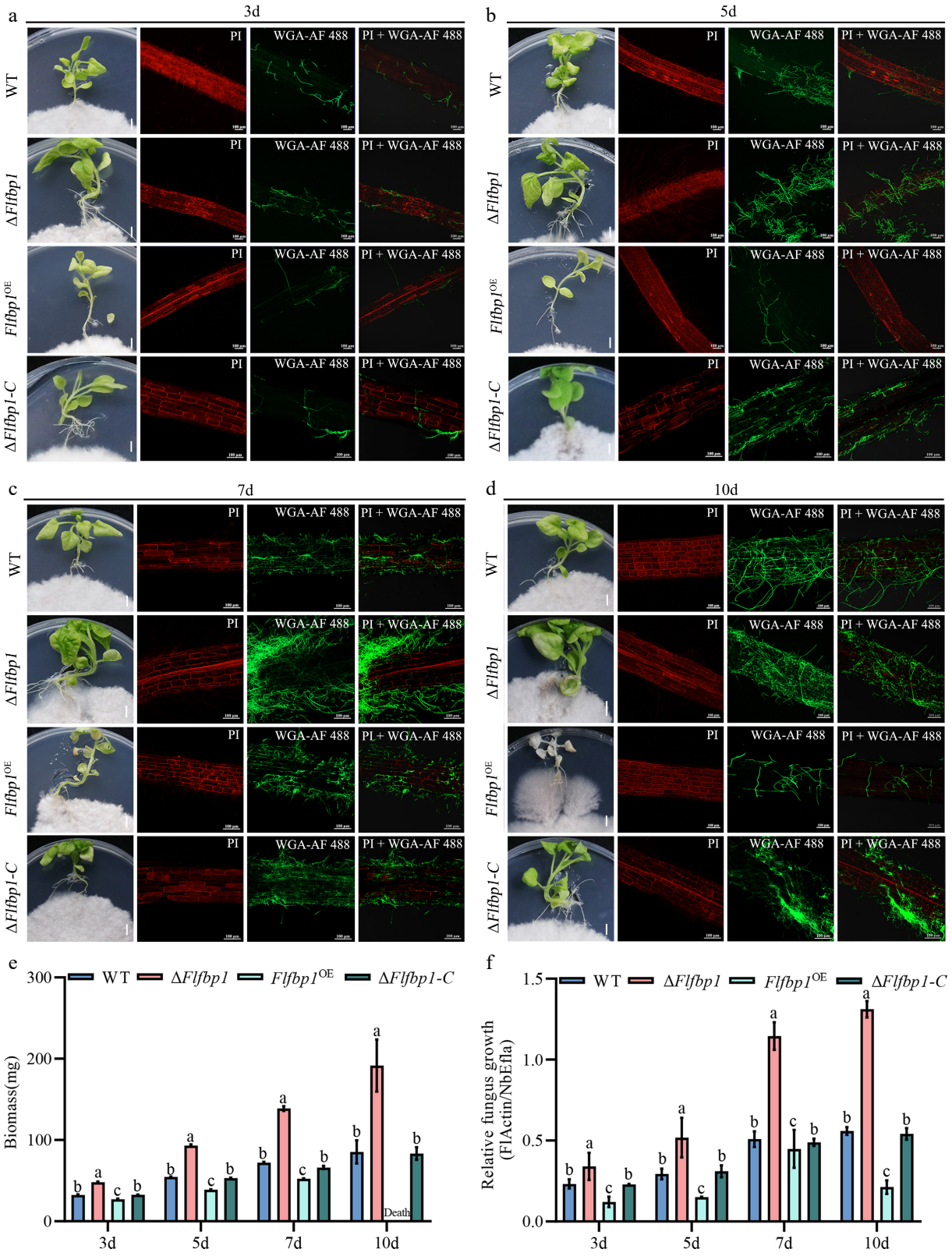

Fig. 2 Flfbp1 mediates the transition from symbiosis to pathogenicity in *F. lateritium* during interaction with *N. benthamiana*. (a)–(d) Interaction phenotypes (left) and laser confocal images of root colonization (right) of *N. benthamiana* inoculated with WT, Δ*Flfbp1*, *Flfbp1*^{OE} strain, or Δ*Flfbp1-C* strain at (a) 3, (b) 5, (c) 7, and (d) 10 d post-inoculation (dpi). Fungal hyphae were visualized by fluorescein-conjugated wheat germ agglutinin (WGA-488, green fluorescence), and plant cell walls were stained with propidium iodide (PI, red fluorescence). Scale bar = 100 μm. The scale in the figure represents 1 cm. (e) Biomass of *N. benthamiana* following inoculation with different strains at 3, 5, 7, and 10 dpi. Values are means ± SD (n = 15 biological replicates). Different lowercase letters indicate significant differences at $p < 0.01$. (f) Relative colonization rate of each strain in *N. benthamiana* roots, determined as the relative DNA ratio of fungal actinto plant EF-1α. Values are means ± SD (n = 3). Different lowercase letters indicate significant differences at $p < 0.01$.

these differentially expressed genes showed that they mainly affected carbohydrate metabolic processes (Supplementary Fig. S7c, S7d). Further analysis of the differentially expressed genes (DEGs) involved in carbohydrate metabolic processes revealed 22 DEGs related to cell wall-degrading enzymes (CWDEs), among which 21 were significantly up-regulated, and 1 was significantly down-regulated (Supplementary Fig. S7e; Table 1). This indicates that Flfbp1 positively regulates the expression of CWDEs in *F. lateritium* Fl617. During plant infection, pathogenic fungi typically activate CWDEs to decompose the plant cell wall—this helps them break through plant defenses, invade tissues, proliferate extensively in plant tissues, and plunder nutrients, ultimately leading to plant death[49]. Meanwhile, plants activate immune responses to restrict the spread of pathogens[50]. We further examined the cell wall integrity of tobacco roots upon 10 d of co-cultivation with WT, Δ*Flfbp1* knockout mutant, and *Flfbp1*^{OE} strains of *F. lateritium* Fl617, using Calcofluor White staining. Host root cell walls displayed continuous fluorescence and intact structure in both the WT and Δ*Flfbp1* treatments, with fungal colonization predominantly occurring on the root surface. By contrast, inoculation with the *Flfbp1*^{OE} strain only marginally compromised host root cell wall integrity, with slight discontinuities in fluorescence detected in localized regions (Supplementary Fig. S8a). Quantitative analysis showed that there was no significant difference in fluorescence intensity between the WT and ΔFlfbp1 strains, whereas the intensity in the *Flfbp1*^{OE} strain was decreased by approximately 2.8% compared with the WT (Supplementary Fig. S8b). Together, these results demonstrate that Flfbp1 exerts only a modest regulatory role in the cell wall-degrading capacity of *F. lateritium* Fl617 during plant infection. Furthermore, further analysis of the fungus–plant interaction transcriptome data showed that after the *Flfbp1*^{OE} strain interacted with tobacco, the transcriptional levels of tobacco genes related to the PTI/ETI pathways (WRKY, LRR, PR, RPS, RPM1, SAG101, NGR1) and the salicylic acid (SA), jasmonic acid (JA), and ethylene (ET) signaling pathways (NPR1, LOX, PAL, AOS, AOC, ERF, DREB) were significantly down-regulated (Supplementary Fig. S9; Table 2). These results indicate that Flfbp1 negatively regulates plant immunity.

Based on the above results, we found a contradiction between Flfbp1 positively regulating CWDEs expression and the observation that overexpression of *Flfbp1* leads to reduced colonization rate of endophytic *F. lateritium* in tobacco, as well as the significant inhibition of plant immune defense reactions by overexpressed *Flfbp1*. We speculated that the up-regulation of CWDEs caused by overexpressed *Flfbp1* may have limited direct contribution to tobacco death, and there may be other factors mediating plant necrosis. Existing research on pathogenic *Fusarium* species, such as *F. oxysporum* and *F. graminearum*, all require a progressive pathogenic mechanism of 'CWDEs establishing colonization foundation-toxins inducing physiological disorders-effector proteins blocking immunity'[51,52]. Since Flfbp1 contributes little to plant death by regulating CWDEs, there must be other causes mediating plant death. Therefore, we focused on the transcription of secondary metabolism-related genes and found that overexpression of *Flfbp1* significantly up-regulates the expression of secondary metabolite biosynthesis genes in *F. lateritium*. Nine secondary metabolite biosynthesis-related genes were differentially expressed, with eight significantly up-regulated and one down-regulated. These genes include not only core functional enzyme genes such as PKS and P450 monooxygenase, but also modifier enzyme genes involved in toxin synthesis (e.g., Pats, pytC, Lac2) (Supplementary Fig. S7f; Table 3). In addition, studies have confirmed that homologs of Flfbp1 have the function of regulating fungal secondary metabolism. For example, the deletion of BcFrp1 in *Botrytis cinerea* inhibits the biosynthesis of ABA[53]. Therefore, we hypothesize that Flfbp1 may also affect plant growth by regulating the secondary metabolites of the endophytic *F. lateritium*.

β-Carboline emerges as a pivotal metabolite governing the symbiotic interplay between endophytic *F. lateritium* and *N. benthamiana*

Based on the above speculation, Flfbp1 may mediate the shift in interaction patterns with plants by regulating the changes in secondary metabolites of the endophytic fungus *F. lateritium* Fl617. To test this hypothesis, we first analyzed the effects of metabolites

Table 1. Analysis of differential genes in the cell wall-degrading enzymes of *F. lateritium* enriched in the transcriptome.

Fusarium lateritium genes	Log_2FC (OE/FL)	GO, EggNOG, and/or NR description	Significant	Regulate
Cell wall-degrading enzymes				
EVM0001149	4.1263422058244	Unsaturated rhamnogalacturonyl hydrolase YesRYesR (Glycosyl Hydrolase Family 88)	Yes	Up
EVM0001588	6.7535321921235	Rhamnogalacturonate lyase C (Polysaccharide lyase family 4)	Yes	Up
EVM0001845	3.395073389	Beta-galactosidase (Glycosyl Hydrolase Family 2)	Yes	Up
EVM0002028	3.7625450042324	Beta-galactosidase A (Glycosyl Hydrolase Family 35)	Yes	Up
EVM0003233	4.3377427051624	Glucoamylase (Glycosyl Hydrolase Family 15)	Yes	Up
EVM0003341	5.9239346913422	Endoglucanase gh5-1 (Glycosyl Hydrolase Family 5)	Yes	Up
EVM0004535	4.5627028709028	Glucoamylase (Glycosyl Hydrolase Family 15)	Yes	Up
EVM0005962	4.8830260775208	Pectate lyase A (Polysaccharide lyase family)	Yes	Up
EVM0006725	4.8568634249429	Endopolygalacturonase NFIA (Glycosyl Hydrolase Family 28)	Yes	Up
EVM0007219	5.8273546342649	Endo-1,4-beta-xylanase D (Glycosyl Hydrolase Family 10)	Yes	Up
EVM0009068	3.4013339063572	Pectate lyase A (Polysaccharide lyase family)	Yes	Up
EVM0009179	4.0518241399204	Pectate lyase plyB (Polysaccharide lyase family)	Yes	Up
EVM0009658	4.8332427745881	Endopolygalacturonase 1 (Glycosyl Hydrolase Family 28)	Yes	Up
EVM0010041	-11.73729611	Sterol 3-beta-glucosyltransferase UGT80A2 (Glycosyl Hydrolase Family 28)	Yes	Down
EVM0011293	4.4366458043154	Exopolygalacturonase X (Glycosyl Hydrolase Family 28)	Yes	Up
EVM0011394	3.9652487427431	Alpha-amylase A (Glycosyl Hydrolase Family 70)	Yes	Up
EVM0011522	3.7271762129361	Glucan endo-1,3-beta-glucosidase A1 (Glycosyl Hydrolase Family 16)	Yes	Up
EVM0011841	6.5107326693398	Endoglucanase type B (Glycosyl Hydrolase Family 6)	Yes	Up
EVM0012220	4.499780736	Exopolygalacturonase B (Glycosyl Hydrolase Family 28)	Yes	Up
EVM0014279	6.3956127005519	Exopolygalacturonase B (Glycosyl Hydrolase Family 28)	Yes	Up
EVM0014424	3.9059208223736	Mannan endo-1,4-beta-mannosidase C (Glycosyl Hydrolase Family 2)	Yes	Up
EVM0014754	3.6856051164499	Acetylxylan esterase A (Carbohydrate Esterase Family)	Yes	Up

https://doi.org/10.48130/mycosphere-0026-0009

Table 2. Analysis of differential genes in the immune response pathway of *N. benthamiana* enriched in the transcriptome.

Nicotiana benthamiana genes	Log_2FC (OE/FL)	GO, EggNOG, and/or NR description	Significant	Regulate
WRKY transcription factor				
NbL01g07860	−1.241673647	WRKY transcription factor 41	Yes	Down
NbL01g15690	−3.593812762	WRKY transcription factor 12	Yes	Down
NbL01g18710	1.105546491	WRKY transcription factor 68	Yes	Up
NbL02g09960	−1.003699269	WRKY transcription factor 6-like	Yes	Down
NbL02g18470	1.741402689	WRKY transcription factor 71	Yes	Up
NbL02g23870	−1.312867524	WRKY transcription factor 3	Yes	Down
NbL03g04040	1.912414484	WRKY transcription factor 71	Yes	Up
NbL05g11960	1.524342816	WRKY transcription factor 71	Yes	Up
NbL07g16620	−2.303755182	WRKY transcription factor 40	Yes	Down
NbL08g18360	−1.161012818	WRKY transcription factor 11	Yes	Down
NbL09g01620	−1.640251489	WRKY transcription factor 40	Yes	Down
NbL09g06220	1.951379137	WRKY transcription factor 72	Yes	Up
NbL10g07700	−2.863361032	WRKY transcription factor 31	Yes	Down
NbL10g19990	1.52314681	WRKY transcription factor 22-like	Yes	Up
NbL10g23550	−2.738797063	WRKY transcription factor 41	Yes	Down
NbL11g17990	−3.360368884	WRKY transcription factor 41	Yes	Down
NbL12g04240	−1.55993108	WRKY transcription factor 6-like	Yes	Down
NbL12g17910	−3.918944509	WRKY transcription factor 31	Yes	Down
NbL13g21070	−2.266601595	WRKY transcription factor 53	Yes	Down
NbL14g00310	−3.921095011	WRKY transcription factor 53	Yes	Down
NbL14g02780	−1.182195457	WRKY transcription factor 11	Yes	Down
NbL14g08830	−1.854152885	WRKY transcription factor 70	Yes	Down
NbL15g14920	2.441100724	WRKY transcription factor 50	Yes	Up
NbL15g22610	1.535103613	WRKY transcription factor 71	Yes	Up
NbL16g10110	1.551883465	WRKY transcription factor 22-like	Yes	Up
NbL17g05520	1.80229719	WRKY transcription factor 50	Yes	Up
NbL17g27990	−2.801993452	WRKY transcription factor 41	Yes	Down
NbL19g03290	2.043828788	WRKY transcription factor 71	Yes	Up
NbL19g12080	1.288989916	WRKY transcription factor 31	Yes	Up
NbL19g15140	−1.751825562	WRKY transcription factor 70	Yes	Down
Leucine-rich repeat receptor-like serine				
NbL02g07080	−1.037744779	Leucine-rich repeat receptor-like serine/threonine-protein kinase BAM1	Yes	Down
NbL03g17050	−1.659993754	LRR receptor-like serine/threonine-protein kinase	Yes	Down
NbL09g04840	−1.971232488	Leucine-rich repeat receptor-like serine/threonine/tyrosine-protein kinase SOBIR1	Yes	Down
NbL11g04700	−1.884686396	Leucine-rich repeat receptor-like serine/threonine/tyrosine-protein kinase SOBIR1	Yes	Down
NbL13g00980	1.004092561	Leucine-rich repeat receptor-like serine/threonine-protein kinase	Yes	Up
NbL13g08970	−2.012289508	LRR receptor-like serine/threonine-protein kinase	Yes	Down
NbL14g11540	−1.442825297	Leucine-rich repeat receptor-like serine/threonine-protein kinase	Yes	Down
NbL15g20260	−1.179377956	Leucine-rich repeat receptor-like serine/threonine-protein kinase	Yes	Down
NbL16g14160	−1.520479646	Leucine-rich repeat receptor-like serine/threonine-protein kinase BAM1	Yes	Down
NbL17g04410	−1.02197164	Leucine-rich repeat receptor-like protein kinase	Yes	Down
NbL19g02860	−1.051309293	Leucine-rich repeat receptor-like serine/threonine-protein kinase BAM1	Yes	Down
NbL04g12340	−1.814698751	Receptor-like protein kinase HSL1	Yes	Down
Pathogenesis-related (PR) proteins				
NbL03g07430	−1.429807222	Nematode resistance protein-like HSPRO2	Yes	Down
NbL16g23530	−1.885653116	Glucan endo-1,3-beta-glucosidase, acidic isoform GI9-like	Yes	Down
NbL16g23540	−3.618771859	Glucan endo-1,3-beta-glucosidase, acidic isoform GI9-like	Yes	Down
NbL07g06460	−2.069325285	Uncharacterized LOC104245359	Yes	Down
NbL16g23610	1.566553502	Uncharacterized LOC107801208	Yes	Up
NbL17g14890	−3.052558899	Uncharacterized LOC104245359	Yes	Down
NbL03g04450	−4.768478445	Transcription factor TCP4-like	Yes	Down
NbL05g09570	−3.201674726	Transcription factor TCP4-like	Yes	Down
NbL09g02150	−4.588823659	Transcription factor TCP4-like	Yes	Down
NbL15g21350	−3.618126068	Transcription factor TCP4-like	Yes	Down
Effector-Triggered Immunity				
NbL00g00160	3.616884706	F-box protein At4g00755-like	Yes	Up
NbL03g23000	−1.203580403	30S ribosomal protein S17	Yes	Down
NbL08g10330	−1.360337605	30S ribosomal protein S13	Yes	Down
NbL13g19700	1.345607674	Uncharacterized LOC107801214	Yes	Up
NbL13g20660	−1.077533904	30S ribosomal protein S17	Yes	Down
NbL13g25880	1.322339361	Uncharacterized LOC105111765	Yes	Up
NbL16g15970	−1.01109948	30S ribosomal protein S1, chloroplastic-like	Yes	Down

(to be continued)

Table 2. (continued)

Nicotiana benthamiana genes	Log_2FC (OE/FL)	GO, EggNOG, and/or NR description	Significant	Regulate
NbL18g08740	−1.493428396	30S ribosomal protein S13	Yes	Down
NbL02g12270	−1.625857953	Uncharacterized LOC109215327	Yes	Down
NbL02g26120	−1.520316021	Uncharacterized LOC109216575	Yes	Down
NbL05g09740	−1.424188808	30S ribosomal protein S20	Yes	Down
NbL10g03010	−1.094115168	Disease resistance protein RPS5-like	Yes	Down
NbL10g06340	1.183761039	40S ribosomal protein S27-2-like	Yes	Up
NbL15g21250	−1.319829734	30S ribosomal protein S20	Yes	Down
NbL05g20820	−4.561840593	Disease resistance protein RPM1-like	Yes	Down
NbL02g11930	−2.326840928	Senescence-associated carboxylesterase 101-like	Yes	Down
NbL00g04260	−4.60786075	Disease resistance protein	Yes	Down
SA/JA				
NbL10g04670	−1.079625198	Phenylalanine ammonia-lyase-like	Yes	Down
NbL12g19650	−1.113061669	Phenylalanine ammonia-lyase	Yes	Down
NbL18g01320	−1.440403027	Negative regulator of resistance-like	Yes	Down
NbL17g18350	−2.193881775	Protein LOL1	Yes	Down
NbL07g15240	2.29744213	9-divinyl ether synthase-like	Yes	Up
NbL07g15260	−2.369372689	9-divinyl ether synthase-like	Yes	Down
NbL17g08900	−1.321601646	Allene oxide synthase	Yes	Down
NbL02g15000	−2.995048075	Allene oxide cyclase, chloroplastic-like	Yes	Down
NbL19g01710	−4.343728998	Allene oxide cyclase 4	Yes	Down
NbL01g10560	1.876627957	Linoleate 9s-lipoxygenase	Yes	Up
NbL03g24390	−2.349266144	Linoleate 13S-lipoxygenase 3-1	Yes	Down
NbL08g01350	−2.350649607	Linoleate 13S-lipoxygenase 2-1	Yes	Down
NbL09g01460	−1.660452484	Haloalkane dehalogenase-like	Yes	Down
NbL13g19150	−2.74590776	Linoleate 13S-lipoxygenase 3-1	Yes	Down
NbL16g03630	−1.315186628	Haloalkane dehalogenase-like	Yes	Down
NbL16g19580	−2.348098997	Linoleate 9S-lipoxygenase 6	Yes	Down
NbL16g25540	−1.222038612	Epoxide hydrolase 3	Yes	Down
NbL03g23910	−1.955594438	Indeterminate-domain 7-like	Yes	Down
NbL05g04140	−1.577936143	Zinc finger protein JACKDAW-like	Yes	Down
NbL05g12780	−1.359270237	TIFY 10A-like	Yes	Down
NbL07g08970	−1.700895662	Indeterminate-domain 5	Yes	Down
NbL08g15780	−1.646076282	Zinc finger protein JACKDAW-like	Yes	Down
NbL09g10490	−1.135563114	Indeterminate-domain 7-like	Yes	Down
NbL09g15900	−1.390531826	Indeterminate-domain 9-like	Yes	Down
NbL09g22330	1.599657779	Uncharacterized LOC104223950	Yes	Up
NbL10g03940	−2.314481352	TIFY 10A-like	Yes	Down
NbL11g03270	−1.648124129	Indeterminate-domain 9-like	Yes	Down
NbL13g19260	−1.439641761	TIFY 10A-like	Yes	Down
NbL13g19660	−1.552337422	Indeterminate-domain 7-like	Yes	Down
NbL17g05190	−1.724278896	Indeterminate-domain 7-like	Yes	Down
NbL17g08700	−1.297468704	Indeterminate-domain 9-like	Yes	Down
NbL17g12750	−1.896400481	Indeterminate-domain 5	Yes	Down
NbL16g09660	−5.012615586	Transcription factor MYC2-like	Yes	Down
Ethylene				
NbL01g02770	−5.903956323	Ethylene-responsive transcription factor ERF109-like	Yes	Down
NbL01g04330	−1.49926367	24-methylenesterol C-methyltransferase 2	Yes	Down
NbL01g07430	2.086831009	1-aminocyclopropane-1-carboxylate synthase	Yes	Up
NbL01g13990	−1.608800619	Reversion-to-ethylene sensitivity1-like	Yes	Down
NbL02g15000	−2.995048075	Allene oxide cyclase, chloroplastic-like	Yes	Down
NbL02g20260	−1.585372911	Ethylene-responsive transcription factor 12-like	Yes	Down
NbL03g03800	−1.138883212	Ethylene-responsive transcription factor 4-like	Yes	Down
NbL03g06570	1.179196435	Dehydration-responsive element-binding protein 2C-like	Yes	Up
NbL03g10380	−1.06543775	Ethylene-responsive transcription factor 5-like	Yes	Down
NbL03g11340	−4.610522757	Dehydration-responsive element-binding protein 1A-like9	Yes	Down
NbL03g21840	−1.010144763	Serine/threonine-protein kinase EDR1-like	Yes	Down
NbL04g09050	1.149021282	Ethylene-responsive transcription factor ABR1-like	Yes	Up
NbL04g09950	−1.184170911	Ethylene-responsive transcription factor RAP2-4-like	Yes	Down
NbL05g17920	−1.838124295	Ethylene-responsive transcription factor 9-like	Yes	Down
NbL05g20110	−1.104123236	AP2/ERF and B3 domain-containing transcription repressor RAV2-like	Yes	Down
NbL06g08080	−1.986073134	Ethylene-responsive transcription factor 4-like	Yes	Down
NbL07g06140	−2.76452384	AP2-like ethylene-responsive transcription factor AIL5	Yes	Down
NbL07g10510	−5.526704793	Dehydration-responsive element-binding protein 1A-like	Yes	Down

(to be continued)

Table 2. (continued)

Nicotiana benthamiana genes	Log_2FC (OE/FL)	GO, EggNOG, and/or NR description	Significant	Regulate
NbL08g01300	1.257845004	Ethylene insensitive 3-like	Yes	Up
NbL08g03410	1.005329917	Ethylene-responsive transcription factor RAP2-7-like	Yes	Up
NbL08g07520	−1.891782173	Ethylene-responsive transcription factor 3-like	Yes	Down
NbL08g09830	−1.160870679	2-methylene-furan-3-one reductase	Yes	Down
NbL08g21280	2.218650596	Ethylene-responsive transcription factor ERF113-like	Yes	Up
NbL09g20840	−1.553979428	Bifunctional protein FolD 2-like	Yes	Down
NbL10g03300	−2.159895802	1-aminocyclopropane-1-carboxylate oxidase 1	Yes	Down
NbL10g05370	−7.38227996	Nicotiana tabacum ethylene-responsive transcription factor ERF027-like	Yes	Down
NbL10g06930	−5.026480543	Ethylene-responsive transcription factor ERF017-like	Yes	Down
NbL10g11290	−1.074701007	Ethylene-responsive transcription factor 5-like	Yes	Down
NbL10g14470	−1.664184862	Ethylene-responsive transcription factor 5-like	Yes	Down
NbL10g19050	−1.863484897	Ethylene-responsive transcription factor 4-like	Yes	Down
NbL10g21330	−5.391660122	Ethylene-responsive transcription factor ERF027-like	Yes	Down
NbL11g19050	−1.208848489	Ethylene-responsive transcription factor 3-like	Yes	Down
NbL11g21170	−7.33308025	Proteinase inhibitor I-B-like	Yes	Down
NbL11g21240	−7.555580287	Proteinase inhibitor I-B-like	Yes	Down
NbL12g20490	−1.178362986	Ethylene-responsive transcription factor RAP2-10-like	Yes	Down
NbL12g22380	−4.49685346	Ethylene-responsive transcription factor ERF106-like	Yes	Down
NbL13g10010	−1.179060632	Ethylene-responsive transcription factor 5	Yes	Down
NbL13g11170	−4.98293508	Dehydration-responsive element-binding protein 1D-like	Yes	Down
NbL13g11180	−5.543553262	Dehydration-responsive element-binding protein 1D-like	Yes	Down
NbL14g02300	2.677049523	Uncharacterized LOC109233752	Yes	Up
NbL14g07490	−4.03320461	Ethylene-responsive transcription factor ERF018-like	Yes	Down
NbL14g20670	−1.508101501	Ethylene-responsive transcription factor RAP2-4-like	Yes	Down
NbL14g21920	−1.534851742	AP2/ERF and B3 domain-containing transcription factor RAV1	Yes	Down
NbL15g00150	−1.338822043	Ethylene-responsive transcription factor 5-like	Yes	Down
NbL15g00610	−3.197292607	Ethylene-responsive transcription factor ERF109-like	Yes	Down
NbL15g12550	1.353059627	Dehydration-responsive element-binding protein 2A-like	Yes	Up
NbL15g23980	−1.2678142	Ethylene-responsive transcription factor 4	Yes	Down
NbL16g02670	−6.459788949	Ethylene-responsive transcription factor ERF017	Yes	Down
NbL16g03200	1.099968315	Ethylene-responsive transcription factor 3-like	Yes	Up
NbL16g03230	−1.50826366	1-aminocyclopropane-1-carboxylate oxidase 1	Yes	Down
NbL16g26030	−1.257999838	Ethylene-responsive transcription factor-like protein	Yes	Down
NbL17g02970	1.392879379	Dehydration-responsive element-binding protein 2A-like	Yes	Up
NbL17g04280	−3.585379082	Dehydration-responsive element-binding protein 3-like	Yes	Down
NbL17g11150	−6.109000485	Ethylene-responsive transcription factor ERF026-like	Yes	Down
NbL17g25900	−3.016530627	Ethylene-responsive transcription factor ERF027-like	Yes	Down
NbL18g01290	1.014692846	Ethylene-responsive transcription factor ERF118-like	Yes	Up
NbL18g09140	−1.069612422	2-methylene-furan-3-one reductase-like	Yes	Down
NbL19g01710	−4.343728998	Allene oxide cyclase 4	Yes	Down
NbL19g04830	1.765903636	Ethylene-responsive transcription factor ERF091	Yes	Up
NbL19g05200	−2.916232465	Ethylene-responsive transcription factor 12-like	Yes	Down
NbL19g15660	2.249205054	Ndehydration-responsive element-binding protein 2B-like	Yes	Up

from different strains on the growth of *N. benthamiana*. The results showed that, at the same concentration, metabolites from the WT strain significantly promoted tobacco growth, with tobacco biomass being 1.43-fold that of the CK ($p < 0.01$) (Supplementary Fig. S10). The growth-promoting activity was further enhanced in the *Flfbp1* knockout mutant (Δ*Flfbp1*), whose metabolites increased tobacco biomass to 4.08-fold relative to the WT strain ($p < 0.01$). Metabolites from the *Flfbp1* complemented strain (Δ*Flfbp1-C*) exhibited a growth-promoting effect similar to that of the WT strain, with no statistically significant difference in tobacco biomass. In contrast, metabolites from the *Flfbp1*^{OE} strain caused lethal effects on tobacco seedlings (Fig. 3a, b). To exclude potential interference from osmotic stress caused by metabolite addition, a NaCl control with an equivalent concentration was included, which showed no obvious effects on tobacco growth (Fig. 3a, b). Together, these results indicate that Flfbp1 may affect the interaction mode between the fungus and its host by modulating fungal metabolite production.

To pinpoint the key secondary metabolites orchestrating the Flfbp1-mediated transition of endophytic *F. lateritium* from symbiosis to pathogenesis, we conducted comparative profiling of the secondary metabolomes in WT and *Flfbp1*^{OE} strains. Our analyses revealed that *Flfbp1* overexpression not only significantly augmented the diversity of secondary metabolite classes but also markedly upregulated the abundance of specific compounds, with a panel of differential metabolites identified (Supplementary Fig. S11a, S11b). It includes differential metabolites such as 4-nitrocatechol, vanillin, and β-Carboline. Existing studies have confirmed that these three substances—4-nitrocatechol, vanillin, and β-Carboline—all possess plant growth-inhibiting activity[54,55,23]. However, among the differential metabolites in this study, β-Carboline exhibits particularly significant content variation. Based on this, β-Carboline was isolated and purified, and its structure was confirmed using high-resolution mass spectrometry (HRMS) and nuclear magnetic resonance (NMR): HRMS (ESI^+) m / z: $[M + H]^+$,

Table 3. Analysis of differential genes in the biosynthesis secondary metabolites of *F. lateritium* enriched in the transcriptome.

Fusarium lateritium genes	Log_2FC (OE/FL)	GO, EggNOG, and/or NR description	Significant	Regulate
Genes for biosynthesis of secondary metabolites				
EVM0000450	4.3614900315927	Cytochrome P450 monooxygenase ATEG	Yes	Up
EVM0002278	4.1569026383141	Laccase-2	yes	up
EVM0005169	3.4262286617577	Fusaridione A synthetase fsdS	Yes	Up
EVM0005566	6.9548778621629	Patulin synthase	Yes	Up
EVM0006747	4.3878350187084	Cytochrome P450 monooxygenase PC-21	Yes	Up
EVM0011686	6.3126194074231	Sterigmatocystin biosynthesis P450 monooxygenase stcS	Yes	Up
EVM0004549	-5.4741035057982	Cytochrome P450 monooxygenase hepE	Yes	Down
EVM0001225	3.51766673868276	Methyltransferase pytC	Yes	Up
EVM0011207	4.75191068032791	ABC transporter G family member 1	Yes	Up

calcd, 169.07625; found, 169.07684 (Supplementary Fig. S11c);^{1}H NMR (500 MHz, $CDCl_3$), $\delta \times 10^{-6}$, (Supplementary Fig. S11d): 7.27–7.30 (q, 1H, phenyl–H, J = 5.0 Hz), 7.54 (s, 1H, phenyl–H), 7.55 (s, 1H, phenyl–H), 7.97 (d, 1H, phenyl–H, J = 5.0 Hz), 8.13 (d, 1H, phenyl–H, J = 10.0 Hz), 8.44 (d, 1H, phenyl–H, J = 5.0 Hz), 8.97 (s, 1H, phenyl–H), 9.81 (s, 1H, –NH); ^{13}C NMR ($CDCl_3$, 126 MHz), $\delta \times 10^{-6}$, (Supplementary Fig. S11e): 111.79, 114.91, 120.05, 121.21, 121.79, 128.68, 129.22, 133.13, 136.04, 138.02, 140.84. The distinct spectral features and mass data unequivocally confirmed the identity of β-Carboline. Given prior reports implicating β-Carboline in plant lethality, we postulated that this compound might mediate processes contributing to plant mortality. Therefore, the content differences and biological functions of β-Carboline were further verified separately. Quantitative analysis revealed that the β-Carboline content in the WT strain was approximately 0.325 mg/g. In the *Flfbp1*^{OE} strain, β-Carboline was markedly accumulated to 3.029 mg/g, which was 9.32-fold higher than that in the WT strain (Fig. 3c). In contrast, the β-Carboline level in the Δ*Flfbp1* mutant was significantly reduced to approximately 0.213 mg/g, accounting for only 65.4% of the WT strain ($p < 0.01$) (Fig. 3c). The β-Carboline content in the Δ*Flfbp1-C* complemented strain was about 0.331 mg/g, showing no significant difference from the WT strain (Fig. 3c). Exogenous application of 0.8 mM β-Carboline demonstrated that β-Carboline significantly inhibited tobacco growth and even caused seedling death (Fig. 3d, e), with the inhibitory effect remarkably enhanced in a concentration-dependent manner (Supplementary Fig. S12).

To identify the biosynthetic source of β-Carboline and rule out the possibility that it is produced by the host plant during fungal–plant interaction, we extracted total secondary metabolites from the interaction systems of tobacco with WT, Δ*Flfbp1*, *Flfbp1*^{OE}, and Δ*Flfbp1-C* strains, and determined β-Carboline contents by high-performance liquid chromatography (HPLC). The results showed that the β-Carboline level in tobacco inoculated with the WT strain was approximately 0.418 mg/g (Fig. 3f). β-Carboline was significantly enriched in the *Flfbp1*^{OE} interaction group, reaching 2.74 mg/g, which was 6.6-fold higher than that in the interaction group of the WT strain and *N. benthamiana* (Fig. 3f). In contrast, the β-Carboline level in the Δ*Flfbp1* interaction group was markedly reduced to approximately 0.149 mg/g, accounting for only 35.65% of that in the interaction group of the WT strain and *N. benthamiana* ($p < 0.01$) (Fig. 3f). The β-Carboline content in the Δ*Flfbp1-C* interaction group was about 0.409 mg/g, showing no significant difference from the WT interaction group (Fig. 3f). Notably, β-Carboline was undetectable in tobacco grown alone (Fig. 3f). To further verify the functional significance of β-Carboline in mediating the fungus–plant symbiotic relationship, exogenous β-Carboline was added to the interaction system of WT and tobacco, adjusting its final concentration to 0.69 mM (this concentration is consistent with that of β-Carboline produced in the interaction system of *Flfbp1* overexpression strain and tobacco). Phenotypic analysis after 10 d of co-cultivation showed that, at this concentration, the growth-promoting effect of the WT strain on tobacco was significantly inhibited, and the biomass of tobacco decreased significantly (Fig. 3g, h). This indicates that β-Carboline is a key substance through which Flfbp1 regulates the symbiosis between endophytic *F. lateritium* and *N. benthamiana*.

Flfbp1 interacts with Flhsp1 and promotes its degradation, likely via ubiquitination

Bioinformatics analysis predicted Flfbp1 as a putative ubiquitin ligase (Fig. 1), and its functions are presumably mediated by protein–protein interactions. To elucidate how Flfbp1 regulates β-Carboline biosynthesis, we performed a Yeast two-hybrid screen and identified Flhsp1 as an interacting partner of Flfbp1 (Fig. 4a). This interaction was subsequently validated using bimolecular fluorescence complementation (BiFC) and co-immunoprecipitation (Co-IP) assays. In the BiFC assay, reconstituted yellow fluorescent signals were detected at the plasma membrane of *N. benthamiana* leaf cells co-expressing Flfbp1-nYFP and *Flhsp1*-cYFP, indicating a potential interaction (Fig. 4b). Consistently, Co-IP analysis using *N. benthamiana* leaves co-expressing Flfbp1-mCherry and Flhsp1-GFP further confirmed their physical interaction (Fig. 4c), consolidating this association.

As previously noted, *Flfbp1* shares high homology with E3 ubiquitin ligases. To dissect the molecular basis of how Flfbp1 acts on Flhsp1, we analyzed the primary structure of Flhsp1 and found that it belongs to the heat shock protein family, containing a ubiquitination site at the 8th amino acid residue (lysine, K) (Fig. 4d). Reports have shown that F-box proteins mainly interact with heat shock proteins (HSPs) through the ubiquitin-proteasome system. This interaction mediates the degradation of HSPs to maintain cellular homeostasis, regulates their chaperone functions, and plays a key role in resisting stress conditions[56]. We next evaluated the protein abundance and ubiquitination level of Flhsp1 in the presence of Flfbp1. Results revealed that Flhsp1 was significantly degraded (approximately 49%) when co-expressed with Flfbp1 (Fig. 4e). However, when we mutate the lysine K at the ubiquitination site of the Flhsp1 protein to arginine R, Flfbp1 is unable to degrade Flhsp1 (Fig. 4d, e). Collectively, these data suggest that Flfbp1 likely acts on Flhsp1 through ubiquitination, with the lysine (K) residue being essential for this process.

Flfbp1-Flhsp1 mediates the transcriptional regulation of Flsmp1 to control β-Carboline biosynthesis

To further elucidate the β-Carboline biosynthetic pathway, we first conducted a literature review and found that the

https://doi.org/10.48130/mycosphere-0026-0009

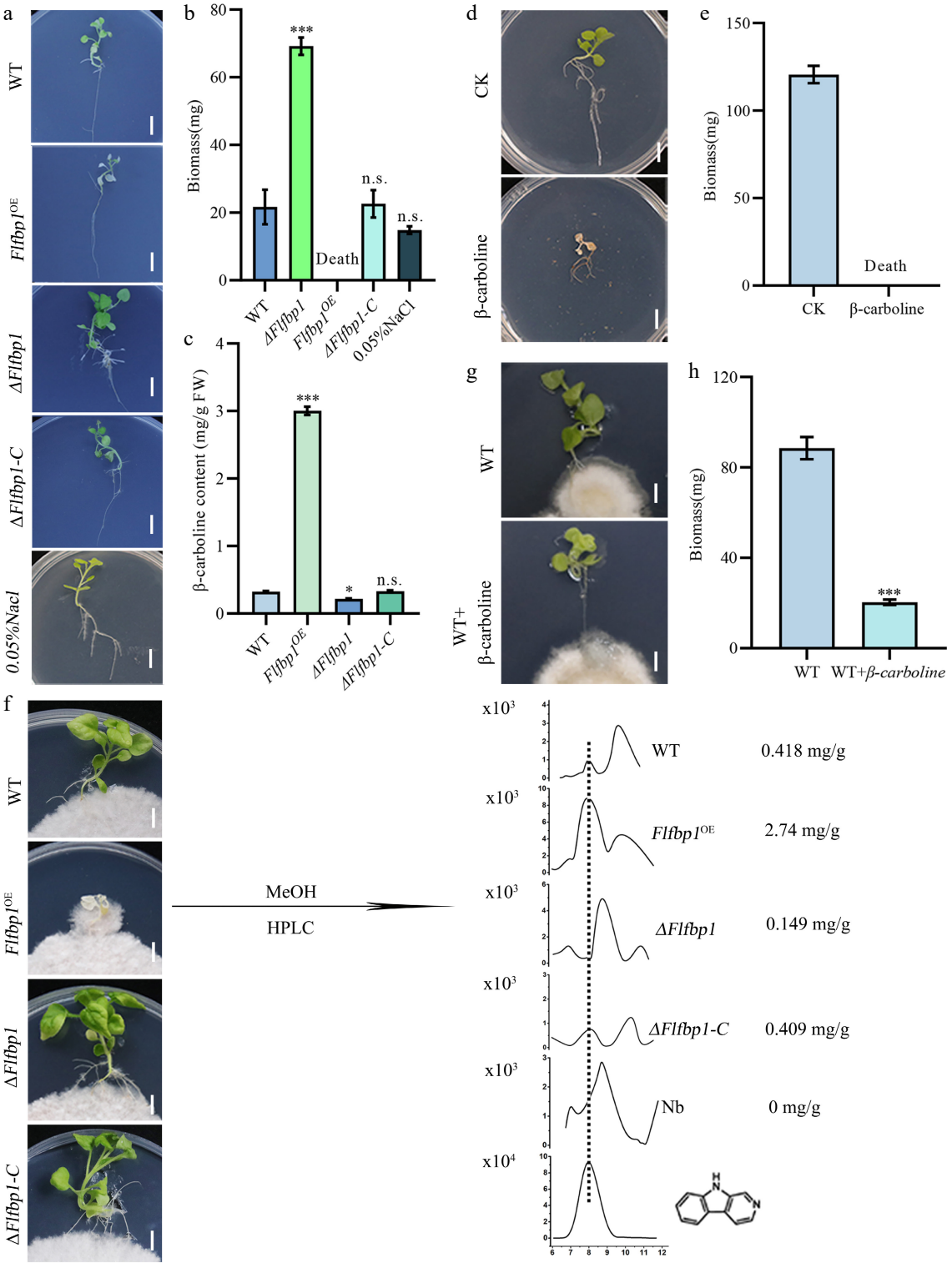

Fig. 3 Flfbp1 controls *β*-Carboline biosynthesis in *F. lateritium* and modulates the growth of *N. benthamiana*. (a) Growth phenotypes of *N. benthamiana* following co-culture with WT, *Flfbp1*^{OE}, Δ*Flfbp1*, and Δ*Flfbp1-C* strains, as well as a 0.05% NaCl control. The scale in the figure represents 1 cm. (b) Biomass quantification of *N. benthamiana* under the indicated treatments. Data are mean ± SD (*n* = 15 biological replicates). 'Death' denotes plant death; n.s. not significant vs WT. (c) *β*-Carboline levels in the indicated fungal strains under pure culture. Data are mean ± SD (*n* = 3). (d) Effects of exogenous *β*-Carboline (800 μM in 0.05% ethanol-containing medium) on *N. benthamiana* growth. Medium supplemented with 0.05% ethanol served as control (CK). Scale bar = 1 cm. (e) Biomass quantification of *N. benthamiana* treated with exogenous *β*-carboline. Data are mean ± SD (*n* = 15 biological replicates). (f) HPLC quantification of *β*-Carbolinein the indicated co-culture systems and *N. benthamiana* alone (Nb). *β*-Carboline contents in WT, *Flfbp1*^{OE}, Δ*Flfbp1*, and Δ*Flfbp1-C* groups were 0.418, 2.74, 0.149, and 0.409 mg/g, respectively, whereas no *β*-Carboline was detected in *N. benthamiana* alone. Bars represent the mean of three biological replicates. (g) Exogenous *β*-Carboline markedly suppresses the plant growth-promoting effect of the WT strain during symbiosis with *N. benthamiana*. (h) Statistics of *N.benthamiana* biomass corresponding to Fig. (g). Data are mean ± SD (*n* = 15 biological replicates). Scale bar = 1 cm. * and *** indicate significant differences relative to WT ($p < 0.01$).

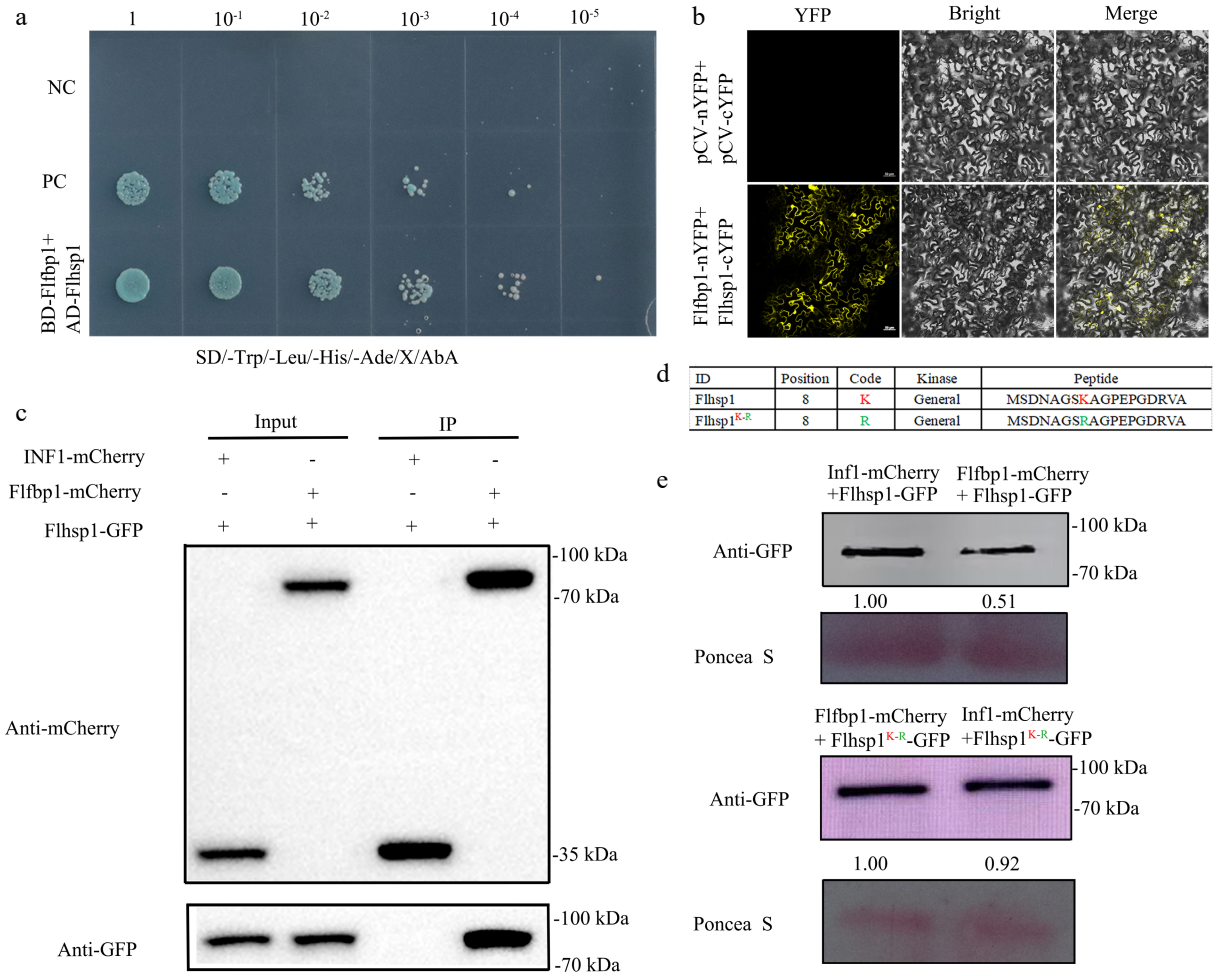

Fig. 4 Flfbp1 interacts with Flhsp1 and regulates its ubiquitination level. (a) Yeast two-hybrid (Y2H) assay verifying the physical interaction between Flfbp1 and Flhsp1. Yeast co-transformed with BD-*Flfbp1* and AD-Flhsp1 grew well and turned blue on SD/-Trp/-Leu/-His/-Ade/X-α-Gal medium. Positive control (PC) showed normal growth, while negative control (NC) showed no growth. (b) Bimolecular fluorescence complementation (BiFC) assay confirming the interaction between Flfbp1 and Flhsp1 in *N. benthamiana* cells. Co-expression of *Flfbp1*-nYFP and *Flhsp1*-cYFP reconstituted yellow fluorescent signals, whereas the empty vector control (pCV-nYFP + pCV-cYFP) showed no fluorescence. (c) Co-immunoprecipitation (Co-IP) assay validating the interaction between Flfbp1 and Flhsp1. *Flfbp1*-mCherry was co-precipitated with *Flhsp1*-GFP in *N. benthamiana*, whereas *INF1*-mCherry used as a negative control showed no interaction with *Flhsp1*-GFP. (d) Prediction of ubiquitination sites in Flhsp1 using the GPS-Uber tool. (e) Flfbp1 regulates the ubiquitination level of Flhsp1. In *N. benthamiana*, Flfbp1 significantly reduced the ubiquitination level of Flhsp1 (relative level = 0.51), whereas INF1 had no such effect. The ubiquitination level of the Flhsp1 ubiquitination-site mutant (K→R) was not affected by Flfbp1 (relative level = 0.92). Protein bands were stained with Ponceau S as a loading control.

Pictet-Spengler reaction is pivotal for constructing the core structure of β-Carboline, specifically the polysubstituted tetrahydroisoquinoline scaffold. Among the enzymes involved, strictosidine synthase, a member of the 'Pictet-Spenglerase' family, functions as a key enzyme in monoterpenoid indole alkaloid biosynthesis[57,58]. Notably, in the bacterial strain *Ralstonia insidiosa*, strictosidine synthase has been identified to regulate the biosynthesis of β-Carboline[59]. In fungi, however, only the biosynthesis of β-Carboline skeletal compounds has been reported, whereas the biosynthetic pathway of β-Carboline itself remains uncharacterized[60]. Through homologous sequence alignment, we identified five homologous proteins of strictosidine synthase in the endophytic fungus *F. lateritium*, among which Flsmp1 showed the highest homology (Fig. 5a). It is speculated that Flsmp1 may be involved in regulating β-Carboline biosynthesis in *F. lateritium* Fl617.

To further dissect the regulatory relationship among Flfbp1, Flhsp1, Flsmp1, and β-carboline, we successfully generated the *Flhsp1* knockout mutant (Δ*Flhsp1*), *Flsmp1* knockout mutant (Δ*Flsmp1*), complemented strains (Δ*Flhsp1-C* and Δ*Flsmp1-C*), and the *Flhsp1* knockout mutant in the *Flfbp1*^{OE} background (*Flfbp1*^{OE}-Δ*Flhsp1*) via targeted gene knockout (Supplementary Fig. S13). We also examined the expression pattern of *Flsmp1* in the Δ*Flfbp1*, *Flfbp1*^{OE}, and WT strains. The results showed that knockout of either *Flfbp1* or *Flhsp1* led to significantly decreased expression of *Flsmp1*, whereas overexpression of *Flfbp1* markedly up-regulated Flsmp1 transcription (Fig. 5b), indicating that *Flsmp1* expression is coordinately regulated by *Flfbp1* and *Flhsp1*. Meanwhile, the growth-promoting effects on tobacco exerted by the Δ*Flhsp1*, Δ*Flsmp1*, and *Flfbp1*^{OE}-Δ*Flhsp1* mutants were significantly stronger than those of the WT strain (Fig. 5c). Tobacco biomass values were 2.81-fold, 2.32-fold, and 2.39-fold higher, respectively, than those of the WT treatment group (Fig. 5d; $p < 0.01$). In contrast, no significant differences in tobacco biomass were observed between the complemented strains and the WT strain (Supplementary Fig. S14). Quantification of β-Carboline revealed that its levels in the interaction systems of Δ*Flhsp1*, Δ*Flsmp1*, and *Flfbp1*^{OE}-Δ*Flhsp1* with plants were significantly reduced to 15.6%, 58.3%, and 33.7% of the WT level, respectively ($p < 0.01$) (Fig. 5e). β-Carboline contents in all complemented

https://doi.org/10.48130/mycosphere-0026-0009

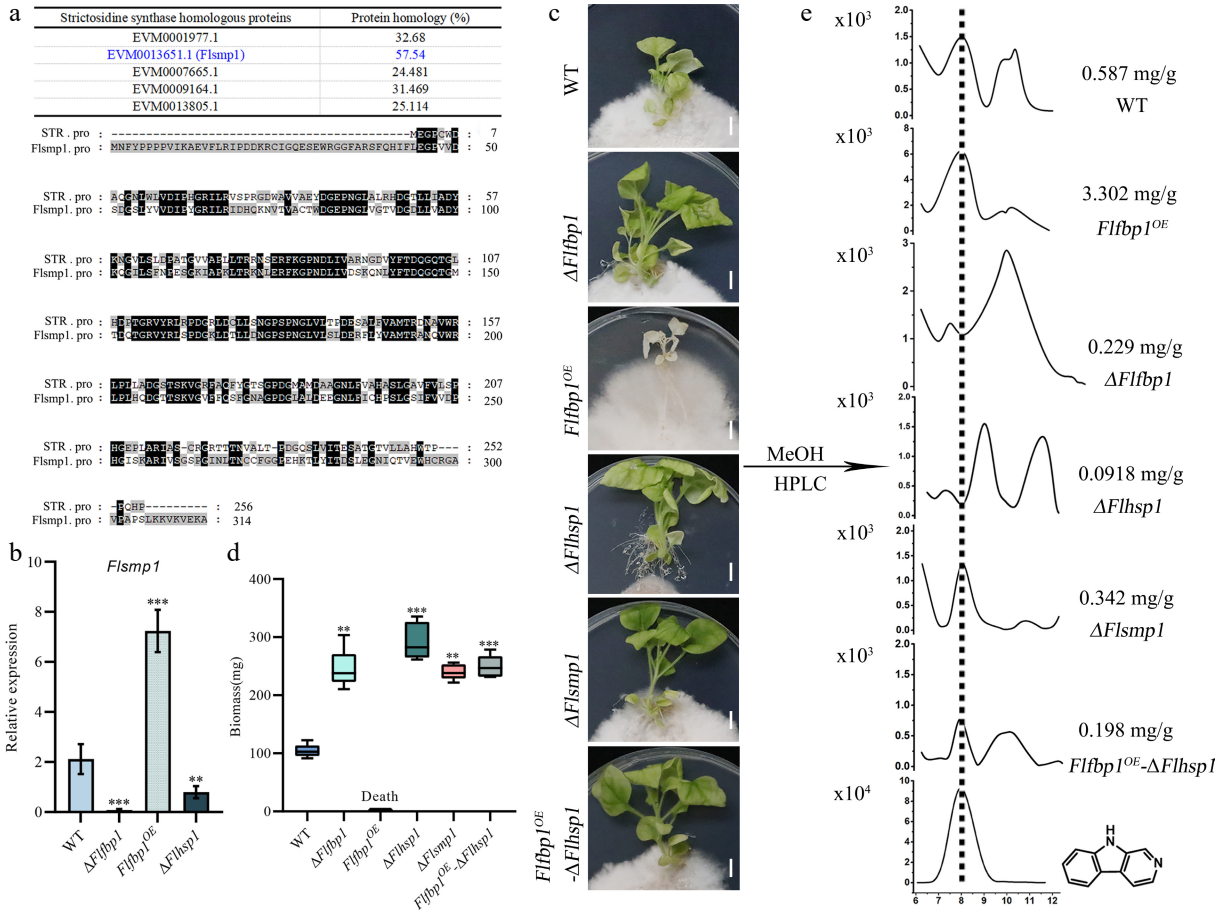

Fig. 5 The *Flfbp1-Flhsp1* module regulates *β*-Carboline biosynthesis by modulating the transcription of *Flsmp1*. (a) Homology alignment of the key *β*-Carboline biosynthesis enzyme (strictosidine synthase homolog) between *Ralstonia insidiosa* FC1138 and *F. lateritium* Fl617. (b) Relative expression levels of *Flsmp1* during the interaction between different fungal strains and *N. benthamiana*. (c) Knockout of *Flhsp1* or *Flsmp1* enhances the plant growth-promoting ability of the fungal strain on tobacco. The scale in the figure represents 1 cm. (d) Quantitative analysis of *N. benthamiana* biomass corresponding to panel (c). Data are means ± SD (n = 15 biological replicates). (e) *β*-Carboline contents in different fungus–tobacco co-culture systems and tobacco alone (*Nb*), determined by HPLC. Data are presented as mean ± SD of three biological replicates. ** and *** indicate significant differences of Δ*Flfbp1*, *Flfbp1*^{OE}, Δ*Flhsp1*, and Δ*Flsmp1* compared with WT ($p < 0.01$).

strains were restored to levels comparable to the WT strain (Supplementary Fig. S14). Collectively, these results suggest that Flfbp1 interacts with Flhsp1 and coordinately modulates the transcription of Flsmp1, thereby regulating the biosynthesis of *β*-Carboline and ultimately mediating the lifestyle transition from endosymbiosis to pathogenicity in the interaction between *F. lateritium* Fl617 and tobacco.

To investigate the functional relationship between Flfbp1 and Flhsp1, we analyzed the growth and sporulation performance of multiple strains, including Δ*Flfbp1*, *Flfbp1*^{OE}, Δ*Flhsp1*, Δ*Flfbp1-C*, Δ*Flhsp1-C*, Δ*Flsmp1*, Δ*Flsmp1-C*, and *Flfbp1*^{OE}-Δ*Flhsp1*, under various stress conditions. All strains, along with the WT control, were cultured on PDA, MS, and MM media supplemented with different stressors at 28 °C under a 12 h light-dark cycle and 60% relative humidity for 7 d. Sporulation rates were determined in 1/4 strength SDB medium. On standard media (PDA, MS, MM) and under various stress conditions, no significant differences in colony morphology, color, or growth rate were observed among WT, Δ*Flfbp1*, Δ*Flsmp1*, and their corresponding complemented strains. In contrast, the *Flfbp1*^{OE} strain exhibited enhanced growth, with significantly larger colony diameters under salt stress and Congo Red-induced cell wall stress ($p < 0.01$) (Supplementary Fig. S15a, S15e, S15f). The Δ*Flhsp1* strain displayed pronounced growth defects across all three media, with colony diameters reduced by 50.4% (PDA), 15.4% (MS), and 40.1% (MM) compared to WT ($p < 0.01$). Growth was further inhibited under salt, acidic (pH 4.0), alkaline (pH 10.4), and oxidative stresses ($p < 0.01$) (Supplementary Fig. S15a–S15i). The growth phenotype of the complemented strain ΔFlhsp1-C was restored to the WT level. Notably, the *Flfbp1*^{OE}-Δ*Flhsp1* mutant exhibited growth defects indistinguishable from Δ*Flhsp1*, indicating that the growth-promoting effect of Flfbp1 overexpression requires a functional Flhsp1. Sporulation assays revealed that the sporulation rates of Δ*Flfbp1*, Δ*Flhsp1*, Δ*Flsmp1*, ΔFlhsp1-C, and *Flfbp1*^{OE}-Δ*Flhsp1* strains were significantly decreased, with the most dramatic reductions observed in the Δ*Flhsp1* strain. In contrast, the sporulation rate of the *Flfbp1*^{OE} strain was significantly increased, while no significant differences were observed between WT, Δ*Flfbp1-C*, and Δ*Flsmp1-C* (Supplementary Fig. S15j). These results demonstrate that both Flfbp1 and Flhsp1positively regulate fungal growth and sporulation, and that the function of Flfbp1 in these processes is dependent on the presence of a functional Flhsp1. Based on these findings and previous studies, we propose that Flfbp1, Flhsp1, and Flsmp1 may constitute a regulatory module involved in beta carboline biosynthesis, modulation of fungus–plant interactions, and control of asexual reproduction. Among them, Flhsp1 appears to play a critical role, as its loss leads to severe defects in both growth

and sporulation, and abolishes the beneficial effects of Flfbp1 overexpression.

Flfbp1-β-Carboline mediates the homeostasis of plant auxins

To investigate the mechanism by which Flfbp1 and β-Carboline inhibit plant growth, we initially analyzed transcriptomic data from fungus–plant interactions. Previous studies have confirmed that the abnormal expression of key regulatory factors in the plant immune system (such as immune signal regulatory genes and resistance-related genes) disrupts the 'activation-inhibition' balance of immune signals, leading to excessive activation of immune pathways and the spread of hypersensitive response (HR) into systemic cell death, thereby inducing plant death[61]. However, our research results show that after treatment with *Flfbp1*^{OE} strains, the transcriptional levels of genes related to PTI/ETI, salicylic acid (SA), jasmonic acid (JA), and ethylene (ET) signaling pathways in tobacco were significantly downregulated (Supplementary Fig. S9; Table 2). This indicates that the plant death induced by *Flfbp1*^{OE} strains is unlikely to be caused by plant immune responses.

Further analysis revealed that *Flfbp1*^{OE} predominantly impacted auxin-related pathways. Among five auxin biosynthesis-associated genes, two were up-regulated, and three were down-regulated, while among 18 auxin transport-related genes, three were upregulated and 15 were down-regulated (Supplementary Fig. S16a, S16b; Table 4). Meanwhile, gibberellin (GA) responsive genes exhibited a down-regulated trend. Among the five GA biosynthesis-related genes, two were up-regulated, and three were down-regulated; among the 10 genes involved in GA perception and signal transduction, two were upregulated, and eight were down-regulated (Supplementary Fig. S17; Table 5). Previous studies have demonstrated that indole-3-acetic acid (IAA) and GA maintain plant hormone homeostasis via a bidirectional synthesis-metabolism regulatory network. Specifically, IAA facilitates GA accumulation by upregulating key GA biosynthesis genes (e.g., GA20ox) and suppressing the activity of GA catabolic enzymes (e.g., GA2-oxidase). In contrast, GA modulates IAA dynamics by enhancing PIN family protein-mediated polar auxin transport and balancing the expression of IAA biosynthesis genes (YUCCA) and catabolic genes (GH3)[62,63]. This interaction network suggests that the regulatory effect of *Flfbp1* on GA-related gene expression is likely an indirect consequence of its interference with the IAA pathway. Accordingly, subsequent studies were focused on the auxin (IAA) signaling pathway. Further analysis revealed that AUX/IAA—a key gene that represses the auxin signaling pathway—was significantly up-regulated, whereas TIR1, the receptor protein gene that activates this pathway, was significantly down-regulated (Supplementary Fig. S16c). These observations collectively suggest that Flfbp1 and β-Carboline may inhibit plant growth by suppressing the auxin signaling pathway in *N. benthamiana*.

To validate this hypothesis, we utilized *Arabidopsis* auxin reporter lines (DR5-GFP and *PIN1pro*:EGFP-GUS) as experimental systems. Phenotypically, knockout mutants (Δ*Flfbp1*, Δ*Flhsp1*, and Δ*Flsmp1*) significantly enhanced plant growth with increased biomass (Fig. 6a, e), whereas the *Flfbp1*^{OE} strain and β-Carboline treatment resulted in plant lethality (Fig. 6b, f). This phenotypic consistency with *N. benthamiana* confirmed the validity of *Arabidopsis* as a model for further mechanistic dissection. Fluorescence analysis of DR5-GFP revealed tissue-specific patterns: no significant differences in fluorescence intensity were observed in root apices across treatment groups, but in the root elongation zone, fluorescence was significantly stronger in the Δ*Flfbp1*, Δ*Flhsp1*, and Δ*Flsmp1* groups compared to the WT. In contrast, no fluorescence signals were detected in the *Flfbp1*^{OE} or β-Carboline-treated groups (Fig. 6c, d). Further analysis using the PIN1pro:GUS reporter system revealed that GUS staining intensity in *Arabidopsis* roots was significantly elevated in the Δ*Flfbp1*, Δ*Flhsp1,* and Δ*Flsmp1* treatment groups, compared to the WT strain control. Conversely, roots treated with *Flfbp1*^{OE} or β-Carboline exhibited significantly reduced GUS staining intensity relative to the WT control (Fig. 6e, g). Additionally, we examined the expression pattern of *AtPIN11* in PIN1pro:EGFP-Gus plants and observed that its expression was significantly upregulated in the Δ*Flfbp1*, Δ*Flhsp1*, and Δ*Flsmp1* treatment groups, whereas it was significantly down-regulated in the *Flfbp1*^{OE} and β-Carboline treatment groups (Fig. 6h). Furthermore, functional validation was performed by exogenously applying 0.69 mM NPA (1-naphthylphthalamic acid), a specific inhibitor of auxin transport, to tobacco seedlings inoculated with the WT strain and the Δ*Flfbp1*, Δ*Flhsp1*, and Δ*Flsmp1* knockout mutants. The results showed that NPA treatment significantly suppressed the growth-promoting effects on tobacco in all inoculation groups (Supplementary Fig. S18a). Notably, under the same NPA treatment, tobacco biomass in the Δ*Flfbp1*, Δ*Flhsp1*, and Δ*Flsmp1* treatment groups remained significantly higher than that in the WT strain treatment group (Supplementary Fig. S18b, S18c). Collectively, these data indicate that Flfbp1 and β-Carboline likely modulate auxin transport rather than biosynthesis, thereby exerting inhibitory effects on plant growth.

Discussion

The stable maintenance of biological order is the core prerequisite for species survival, and this rule applies to all biological communities, including the plant–microbe symbiosis system. The seemingly stable endophyte-plant symbiotic relationship is essentially the result of hundreds of millions of years of interspecific interaction and evolutionary dynamic equilibrium, and the switching of the interaction state between the two parties relies on the driving of core regulatory factors[1,2]. In this study, we took the endophytic *F. lateritium* Fl617 as the research object and identified the ubiquitin E3 ligase F-box protein Flfbp1 as the key regulator mediating the transition between symbiotic and pathogenic states of this strain. We systematically analyzed the molecular mechanism by which Flfbp1, as the core regulator, controls the biosynthesis of β-Carboline, a plant growth inhibitor. Combined with the analysis of fungal cell wall-degrading enzyme profiles and metabolite detection results, we improved the regulatory network of fungus–plant interaction. This study reveals the pathogenic pathway by which β-Carboline hijacks plant auxin transport and leads to plant death, clarifies the functional adaptive evolutionary characteristics of the F-box protein family in endophytic and pathogenic fungi, and provides a new molecular perspective for in-depth understanding of the dynamic balance of microbe–host interactions.

Virulence factors represent the core pathogenic molecules that drive plant death upon infection by pathogenic fungi. Post-translational regulation of virulence factor stability serves as a critical switch governing the transition between pathogenic and symbiotic lifestyles, and the ubiquitin–proteasome pathway constitutes the central regulatory module for this process[64]. Among its components, Fbp1—the substrate-recognition subunit of the E3 ubiquitin ligase—functions as a central regulator of pathogenicity in diverse fungal pathogens, including *F. graminearum* and *F. oxysporum*. This protein is strongly induced during host infection and promotes fungal invasion and colonization by modulating the

https://doi.org/10.48130/mycosphere-0026-0009

Table 4. Analysis of differential genes in auxin pathway of *N. benthamiana* enriched in transcriptome.

Nicotiana benthamiana gene	Log_2FC (OE/FL)	GO, EggNOG, and/or NR description	Significant	Regulate
Transport inhibitor response 1 (TIR1)/auxin signaling F-BOX (AFB) auxin receptor protein				
NbL09g14830	−1.484840014	Transport inhibitor response 1-like	Yes	Down
NbL18g05140	−0.122866608	Auxin signaling F-BOX 2-like	No	Down
NbL18g05510	−0.329982688	Auxin signaling F-BOX 2-like	No	Down
indole-3-acetic acid-amido synthetase				
NbL01g07800	−1.908802784	Indole-3-acetic acid-amido synthetase GH3.5	Yes	Down
NbL02g06310	1.439623697	Indole-3-acetic acid-amido synthetase GH3.1	Yes	Up
NbL05g17320	−1.09617348	Indole-3-acetic acid-amido synthetase GH3.1	Yes	Down
NbL11g18650	−1.114444544	Indole-3-acetic acid-amido synthetase GH3.6-like	Yes	Down
NbL17g22680	1.189671596	Indole-3-acetic acid-amido synthetase GH3.1	Yes	Up
Auxin transporter protein				
NbL01g00650	−4.828880997	Auxin transporter-like protein 2	Yes	Down
NbL03g07460	2.285286635	Auxin transporter-like protein 2	Yes	Up
NbL09g23290	−5.54548812	Auxin transporter-like protein 2	Yes	Down
NbL11g14560	−3.364388709	Auxin transporter-like protein 2	Yes	Down
NbL14g19160	−1.806469884	Auxin transporter-like protein 3	Yes	Down
NbL19g07760	−2.73623543	Regulation of auxin polar transport	Yes	Down
NbL16g18860	−1.150471952	Regulation of auxin polar transport	Yes	Down
NbL14g08500	1.465737757	Protein PIN-LIKES 6-like	Yes	Up
NbL10g12990	−1.623008847	Protein PIN-LIKES 7	Yes	Down
NbL08g15120	1.065093528	Protein PIN-LIKES 6-like	Yes	Up
NbL06g09580	−2.679347268	Protein PIN-LIKES 7	Yes	Down
NbL02g24270	−2.163781867	ABC transporter B family member 19	Yes	Down
NbL19g09930	−1.942374526	ABC transporter B family member 19	Yes	Down
NbL00g02570	−4.828880997	Auxin efflux carrier component 7-like (PIN3)	Yes	Down
NbL04g04410	2.285286635	Auxin efflux carrier component 3-like (PIN3)	Yes	Down
NbL09g07200	−5.54548812	Auxin efflux carrier component 6-like (PIN6)	Yes	Down
NbL16g17760	−3.364388709	Auxin efflux carrier component 1-like (PIN1)	Yes	Down
NbL18g00130	−1.806469884	Auxin efflux carrier component 7-like (PIN3)	Yes	Down
Auxin responsive protein				
NbL01g09250	−1.054583065	Auxin-responsive protein IAA16	Yes	Down
NbL01g21870	−2.523692106	Auxin-responsive protein IAA13-like	Yes	Down
NbL01g23060	−2.440189948	Auxin-responsive protein IAA4	Yes	Down
NbL01g23080	−2.205581671	Auxin-responsive protein IAA7-like	Yes	Down
NbL03g13570	1.429065824	Auxin-responsive protein SAUR32-like	Yes	Up
NbL05g19690	−3.29660792	Auxin-responsive protein SAUR68-like	Yes	Down
NbL07g04240	−5.968493708	Auxin-responsive protein IAA29-like	Yes	Down
NbL08g03870	−3.919578223	Auxin-responsive protein SAUR68-like	Yes	Down
NbL09g00020	−2.628425635	Auxin-responsive protein IAA4-like	Yes	Down
NbL09g00030	−1.626709574	Auxin-responsive protein IAA14-like	Yes	Down
NbL11g16610	−1.400905548	Auxin-responsive protein IAA16	Yes	Down
NbL11g21040	−2.179973728	Auxin-responsive protein IAA4	Yes	Down
NbL11g21050	−1.252856512	Auxin-responsive protein IAA7-like	Yes	Down
NbL13g13620	1.298520512	Auxin-responsive protein SAUR32-like	Yes	Up
NbL13g20890	2.003292672	Auxin-responsive protein IAA17-like	Yes	Up
NbL13g26840	−2.368881964	Auxin-responsive protein SAUR68-like	Yes	Down
NbL13g26870	−4.278233719	Auxin-responsive protein SAUR68-like	Yes	Down
NbL14g07010	−3.567600595	Auxin-responsive protein IAA14	Yes	Down
NbL16g01650	−1.876347783	Auxin-responsive protein IAA27-like	Yes	Down
NbL16g12950	−2.088996357	Auxin-responsive protein IAA13-like	Yes	Down
NbL17g06370	−4.71703058	Auxin-responsive protein IAA29-like	Yes	Down
NbL17g08960	−2.483252353	Auxin-responsive protein SAUR68-like	Yes	Down
NbL17g14080	1.059526377	Auxin-responsive protein SAUR71-like	Yes	Up
NbL18g02000	−4.444820436	Auxin-responsive protein SAUR68-like	Yes	Down
Auxin response factor				
NbL05g12860	−1.083493124	Auxin response factor 19-like	Yes	Down
NbL07g00920	−2.617378332	Auxin response factor 4	Yes	Down
NbL10g04280	−1.315801096	Auxin response factor 1-like	Yes	Down
NbL10g04590	−3.310667496	Auxin response factor 16-like	Yes	Down
NbL10g07900	−1.052066843	Auxin response factor 19-like	Yes	Down
NbL10g23910	−1.512927065	Auxin response factor 9-like	Yes	Down
NbL12g18280	−1.392296468	Auxin response factor 19-like	Yes	Down
NbL17g08330	−1.55076215	Auxin response factor 4	Yes	Down
NbL17g24940	1.292835226	Auxin response factor 5-like	Yes	Up

Table 5. Analysis of differential genes in GA pathway of *N. benthamiana* enriched in transcriptome.

Nicotiana benthamiana gene	Log_2FC (OE/FL)	GO, EggNOG, and/or NR description	Significant	Regulate
GA synthetase				
NbL01g06920	2.280511162	Gibberellin 20-oxidase-like protein	Yes	Up
NbL03g22250	1.169536118	Transcription factor DIVARICATA-like	Yes	Up
NbL07g07470	−1.995380527	Ent-kaur-16-ene synthase	Yes	Down
NbL07g10520	−3.238743936	Gibberellin 20 oxidase 1-like	Yes	Down
NbL19g12570	−1.932379575	Transcription factor DIVARICATA-like	Yes	Down
GA perception and signal transduction protein				
NbL02g07220	1.131961551	Gibberellin receptor GID1B-like	Yes	Up
NbL03g17990	−3.146397875	Gibberellin-regulated protein 1-like	Yes	Down
NbL04g08050	−1.487927675	Gibberellin-regulated protein 9-like	Yes	Down
NbL09g01800	−2.212289988	Scarecrow-like protein 21	Yes	Down
NbL09g12800	−3.619699869	Gibberellin-regulated protein 6-like	Yes	Down
NbL11g08070	−1.674741687	Scarecrow-like protein 21	Yes	Down
NbL13g08210	−5.512312894	Gibberellin-regulated protein 6	Yes	Down
NbL14g18570	−2.055725221	Gibberellin-regulated protein 9-like	Yes	Down
NbL15g20270	1.625391735	Scarecrow-like protein 21	Yes	Up
NbL16g05100	−3.904334877	Gibberellin-regulated protein 6-like	Yes	Down
GA related metabolic protein				
NbL11g20260	−1.525057496	Gibberellin 2-beta-dioxygenase 2-like	Yes	Down
NbL05g10730	−1.760610284	Gibberellin 2-beta-dioxygenase 2-like	Yes	Down
NbL08g06380	1.322026732	Gibberellin 2-beta-dioxygenase 2-like	Yes	Up
NbL16g11350	−3.972446266	gibberellin 2-beta-dioxygenase 2-like	Yes	Down

expression of genes encoding cell wall-degrading enzymes such as cellulases and pectinases, thereby dismantling the plant cell wall barrier. Their pathogenicity strictly relies on the fungal colonization level in the host, which is a classic pathogenic characteristic of pathogenic fungi[11,47,48]. In contrast, our study reveals that the F-box protein Flfbp1 from the endophytic fungus *F. lateritium* Fl617 has undergone pronounced functional divergence. During symbiotic interactions with tomato and *N. benthamiana*, Flfbp1 is stably expressed at low levels and significantly promotes plant growth, while the fungus maintains low cell wall-degrading enzyme activity (Supplementary Figs S1, S2, and S7). Upon overexpression of *Flfbp1*, despite a moderate increase in cell wall-degrading enzyme activity (Supplementary Fig. S7), fungal colonization in planta is drastically reduced, yet the strain triggers host plant death (Fig. 2). These findings establish Flfbp1 as a molecular switch controlling the symbiosis–pathogenicity transition in this endophyte, and demonstrate that cell wall-degrading enzymes are not the primary determinants of its pathogenicity. Intriguingly, this phenomenon is inconsistent with the classical mechanism of pathogenic fungi, in which cell wall-degrading enzymes mediate colonization, and colonization level determines pathogenicity. This finding suggests that this endophytic fungus has evolved a pathogenic pathway independent of colonization density, distinct from the canonical pathogenic mode. In support of this conclusion, metabolic profiling (Figs 3, 5; Supplementary Fig. S11) showed that metabolites from the Δ*Flfbp1* mutant strongly enhance plant growth, whereas metabolites from the *Flfbp1*^{OE} strain directly induce plant death (Fig. 3). These results further confirm that the Flfbp1-mediated lifestyle transition in this endophyte depends primarily on the regulation of specialized metabolite biosynthesis, rather than on cell wall-degrading enzyme activity.

Building on the key regulatory insights from metabolite profiling, we further dissected the core metabolic pathways governed by Flfbp1 and uncovered that secondary metabolites act as a central player in the interaction of this endophytic fungus. Secondary metabolites serve as critical virulence determinants in pathogenic *Fusarium* species. Canonical mycotoxins, including fumonisins, deoxynivalenol, and fusaric acid, induce plant death by directly damaging host cells and suppressing physiological processes, representing the core pathogenic molecules of pathogenic *Fusarium*[65–67]. In contrast, integrated metabolomic and LC-MS analyses (Supplementary Fig. S11) revealed that none of the above-mentioned classic *Fusarium* virulence factors were detected in *F. lateritium* Fl617. Instead, we identified multiple metabolites with plant growth-regulatory activity, such as β-Carboline and 4-nitrocatechol, indicating that this endophytic *F. lateritium* Fl617 employs a novel metabolite system relying on non-canonical virulence factors to modulate host interactions. β-Carboline is a well-characterized alkaloid that regulates plant physiology. Prior studies have only documented its presence in plants and bacteria, together with its plant growth-inhibitory activity, yet its biosynthetic pathway has remained unresolved. A key breakthrough of this study is the first identification of β-Carboline biosynthetic capacity in a *Fusarium* species, and the delineation of its biosynthetic pathway directly controlled by Flfbp1. Mechanistically, Flfbp1 interacts with the heat shock protein Flhsp1 to modulate the transcription of the key gene Flsmp1, thereby precisely governing β-Carboline biosynthesis (Figs 3, 5). Notably, this pathway also raises important unresolved questions. Bioinformatic prediction suggested that Flhsp1 localizes to the cytoplasm and plasma membrane, whereas experimental evidence demonstrated that it exclusively localizes to the plasma membrane (Fig. 4), a pattern distinct from the canonical cytoplasmic localization of conventional HSP70 proteins. The molecular mechanism and biological significance underlying this unique subcellular localization warrant further in-depth investigation.

To verify the central role of the Flfbp1–Flhsp1–Flsmp1 module in regulating the β-Carboline biosynthetic pathway, we performed a series of functional assays using gene knockout, overexpression, and complementation strains. Deletion of any single gene—*Flfbp1*, *Flhsp1*, or *Flsmp1*—resulted in a significant reduction in β-Carboline production (Figs 3, 5) and a pronounced enhancement of plant growth-promoting effects. In contrast, β-Carboline levels were drastically elevated in the *Flfbp1*^{OE} strain (Fig 3), which directly induced host death in tobacco. To exclude non-specific effects such as random insertion and background adaptation during genetic manipulation, we generated complementation strains for

https://doi.org/10.48130/mycosphere-0026-0009

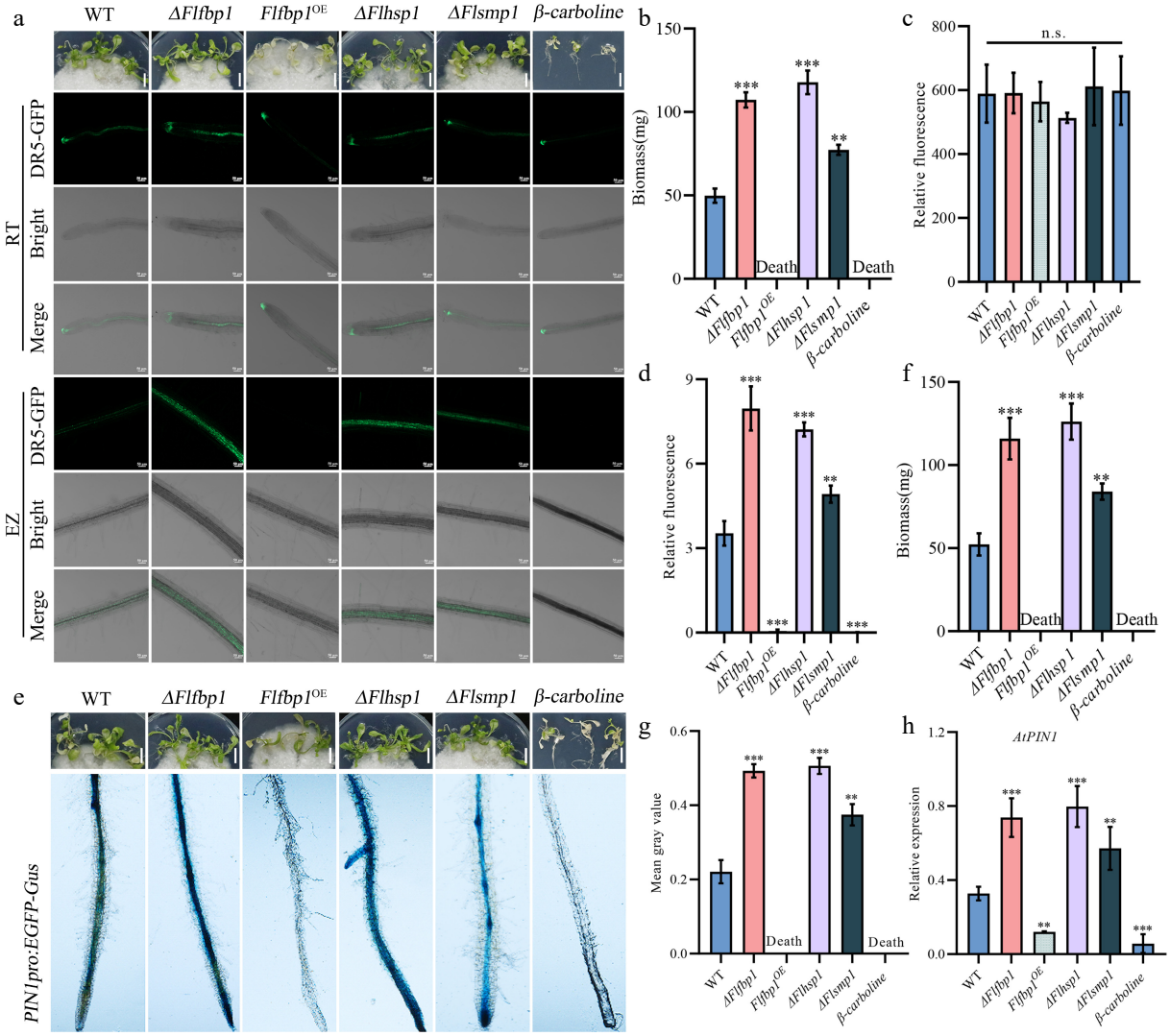

Fig. 6 Mechanistic analysis of Flfbp1 and β-Carbolinein regulating auxin transport in *Arabidopsis thaliana*. (a) Phenotypic effects of different *F. lateritium* strains and β-Carboline treatment on the *Arabidopsis thaliana* DR5-GFP auxin reporter line. The scale in the figure represents 1 cm. (b) Quantitative analysis of *Arabidopsis thaliana* biomass corresponding to panel (a). (c) Quantification of DR5-GFP fluorescence intensity in *Arabidopsis thaliana* root tips shown in panel (a). (d) Quantification of DR5-GFP fluorescence intensity in the elongation zone (EZ) of *Arabidopsis thaliana* root tips shown in panel (a). (e) Effects of different *F. lateritium* strains and β-Carboline treatment on the *Arabidopsis thaliana PIN1pro*:EGFP-GUS line. The scale in the figure represents 1 cm. (f) Quantitative analysis of *Arabidopsis thaliana* biomass corresponding to panel (e). (g) Quantitative analysis of GUS staining gray value in *Arabidopsis thaliana* roots shown in panel (e). (h) Relative expression level of *AtPIN1* under the co-culture of different fungal strains with *Arabidopsis thaliana*. Data are presented as mean ± SD of three biological replicates. ** and *** indicate significant differences of Δ*Flfbp1*, Δ*Flhsp1*, Δ*Flsmp1*, and *Flfbp1*^{OE} compared with WT ($p < 0.01$). Scale bar = 50 μm.

Flfbp1, *Flhsp1*, and *Flsmp1* (Δ*Flfbp1-C*, Δ*Flhsp1-C*, Δ*Flsmp1-C*). These complemented strains restored β-Carboline production to WT strains' levels, and the corresponding growth-promoting or pathogenic phenotypes on tobacco were also restored to the WT state (Figs 3, 5; Supplementary Fig. S14). Collectively, these results demonstrate that β-Carboline acts in a dose-dependent manner to dictate the interaction mode between *F. lateritium* and its host. Low levels support a symbiotic and growth-promoting state, whereas high levels trigger a pathogenic lifestyle. Our data further confirm that the Flfbp1–Flhsp1–Flsmp1 pathway constitutes the core molecular module governing β-Carboline biosynthesis and thereby mediates the symbiosis–pathogenicity switch in *F. lateritium*, while cell wall-degrading enzymes play only a secondary and supportive role in this process.

After defining the core metabolic pathway regulated by Flfbp1, we further identified the host pathogenic molecular targets of this endophyte and found that its pathogenic mechanism bypasses the plant immune pathway. The pathogenic mechanisms of traditional pathogenic fungi are centered on host immune responses, which typically trigger excessive immune reactions and cell death by activating the plant PTI/ETI immune pathways and elevating levels of defense-related hormones such as SA/JA/ET, representing the classic model of plant–pathogen interactions[68,69]. In contrast, our study revealed that after tobacco plants were treated with the *Flfbp1*^{OE} strain, key genes in the host PTI/ETI immune pathways and SA/JA/ET hormone levels were significantly down-regulated. These results ruled out the possibility that plant death was caused by immune responses, confirming that this endophytic fungus bypasses the host immune pathway and instead achieves pathogenicity by directly interfering with the core plant growth regulatory pathway—a key feature that distinguishes it from typical pathogenic fungi (Supplementary Figs S8, S16). Transcriptomic analysis further

identified the core molecular target of this pathogenic process as the plant auxin transport system. Following treatment with the *Flfbp1*^{OE} strain, auxin-responsive genes in tobacco were markedly down-regulated, AUX/IAA family genes (auxin signaling repressors) were up-regulated, and expression of the auxin receptor gene TIR1 was inhibited, ultimately blocking host auxin transport (Supplementary Fig. S16). Functional verification using *Arabidopsis* DR5-GFP and *PIN1pro*:EGFP-Gus lines further confirmed that *β*-Carboline is the direct effector molecule mediating this process (Fig. 6). Thus, Flfbp1 directly targets the plant auxin transport system by regulating *β*-Carboline biosynthesis, interfering with normal host auxin signaling, and ultimately triggering plant death. Consistent with the dose-dependent regulatory pattern of *β*-carboline, low levels of *β*-Carboline do not affect normal auxin transport, allowing the fungus and plant to maintain a symbiotic and growth-promoting relationship. In contrast, high levels of *β*-Carboline strongly inhibit plant auxin transport, disrupt the host's core growth regulatory pathway, and ultimately trigger a pathogenic response (Fig. 7).

This study establishes the Flfbp1-mediated bistable regulatory mechanism in the endophytic fungus *F. lateritium* Fl617. However, several important scientific questions remain to be addressed, pointing to key directions for future research. First, although Flfbp1 acts as a molecular switch governing the symbiosis–pathogenicity transition in this endophyte, the precise regulatory mechanisms that trigger this switch remain to be elucidated. Second, Flhsp1 functions as a critical regulator of *β*-Carboline biosynthesis, yet the molecular basis underlying its exclusive plasma membrane localization is unclear. The detailed interaction mode and binding interface between Flhsp1 and Flfbp1 also require further validation by protein–protein interaction assays. Third, within the Flfbp1-mediated ubiquitination system, it remains unknown whether additional interacting proteins exist beyond Flhsp1. How this module coordinately regulates *β*-Carboline biosynthesis and cell wall-degrading enzyme activity requires further mechanistic dissection. Fourth, the direct molecular target of *β*-Carboline within the plant auxin transport system has not been identified. The binding characteristics and regulatory mechanisms between *β*-Carboline and PIN family transporters warrant in-depth investigation. Fifth, Flfbp1-mediated pathogenicity displays remarkable host specificity: infection leads to lethality in tobacco and *Arabidopsis* but only growth inhibition in tomato. The molecular basis underlying this host specificity, including host recognition elements and divergent signaling pathways, represents a central question in understanding endophyte–host specificity and requires systematic characterization.

In summary, this study reveals the core bistable regulatory mechanism of the endophytic fungus *F. lateritium* Fl617. As the central regulator, Flfbp1 mediates the transcriptional expression of Flsmp1 by interacting with the heat shock protein Flhsp1, thereby achieving dose-dependent regulation of *β*-Carboline biosynthesis. Meanwhile, it modulates cell wall-degrading enzyme activity to play an auxiliary role. As the key effector molecule, *β*-Carboline targets the plant auxin transport system and interferes with the host's core growth regulatory pathway, thereby mediating the transition between symbiotic and pathogenic states in the fungus–plant interaction. The innovations of this study are as follows: we identified the biosynthetic capability of *β*-Carboline in fungi for the first time and elucidated its molecular biosynthetic pathway; we revealed the

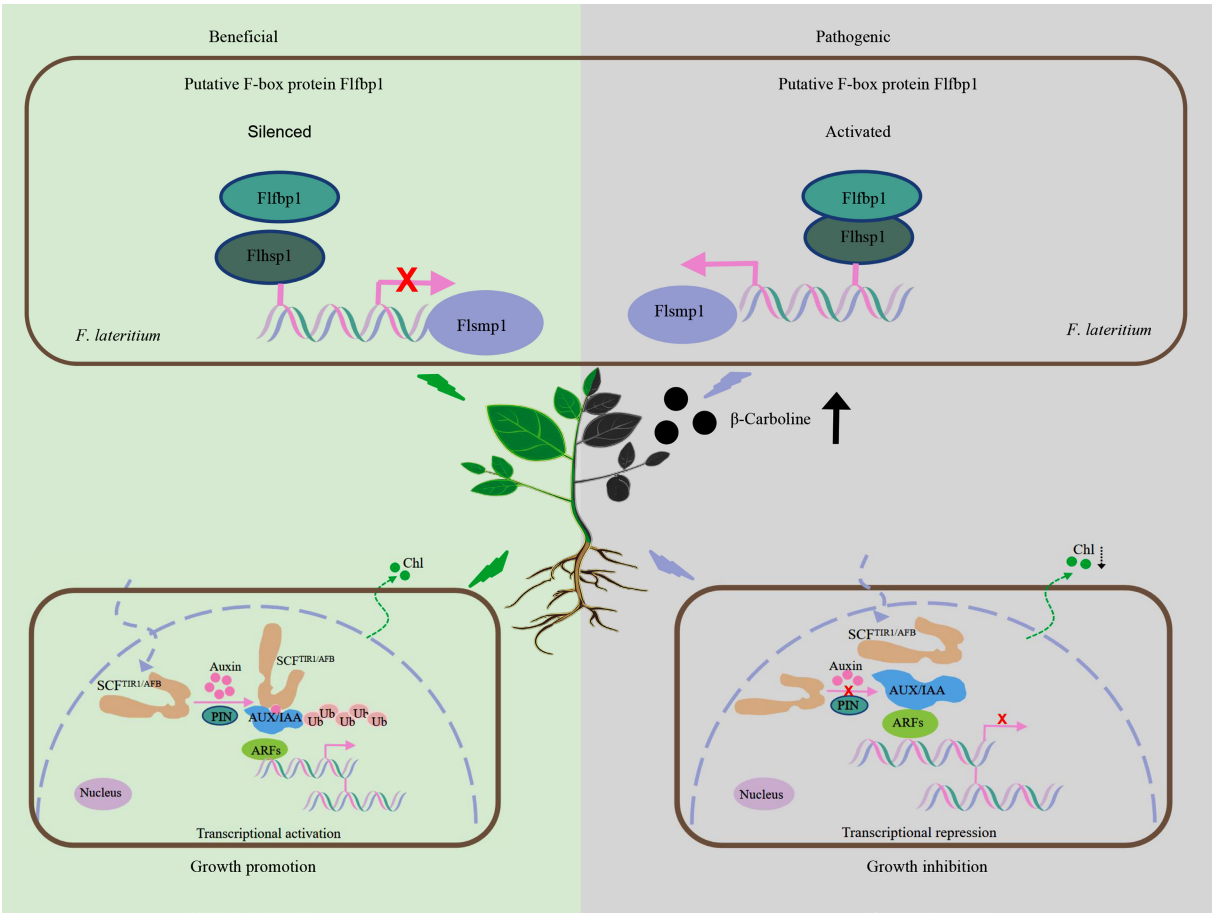

Fig. 7 A model illustrating *F. lateritium* Fl617 state transition (beneficial to pathogenic) regulating plant growth via *β*-Carboline and auxin signaling.

functional adaptive evolution of the F-box protein family between endophytic and pathogenic fungi; and, combined with cell wall-degrading enzyme analysis, we uncovered a pathogenic strategy in endophytic fungi that is immune-independent, colonization-unrelated, and dominated by secondary metabolites with cell wall-degrading enzymes as auxiliary factors. This study not only provides a new model for dissecting the molecular basis of state plasticity in endophytic fungi, but also offers a novel perspective for understanding the dynamic balance of microbe–host interactions. Furthermore, it provides key gene targets and a theoretical foundation for the application of endophytic fungi in the biological control of plant diseases and crop growth promotion.

Author contributions

The authors confirm their contributions to the paper as follows: conceptualization, methodology, data curation, writing – original draft: Li Y; investigation: Zha X, Xiao Q, Wang J, Liu G, Liu R, He Y; conceptualization, methodology, supervision: He Z, Kang J. All authors reviewed the results and approved the final version of the manuscript.

Data availability

All data generated or analyzed during this study are included in this published article and its supplementary information files.

Acknowledgements

Many thanks to the National Natural Science Foundation of China (32160667, 32170019, 31901947 and 32460007) for support of this work. The authors express their sincere gratitude to Professor Daohong Jiang from Huazhong Agricultural University and Professor Fengquan Liu from Guizhou University for their constructive feedback and valuable suggestions regarding this paper.

Conflict of interest

The authors declare no conflict of interest.

Supplementary information accompanies this paper online at: https://doi.org/10.48130/mycosphere-0026-0009.

Dates

Received 25 February 2026; Revised 12 April 2026; Accepted 27 April 2026; Published online 10 July 2026

References

[1] Hiruma K, Aoki S, Takino J, Higa, T, Utami YD, et al. 2023. A fungal sesquiterpene biosynthesis gene cluster critical for mutualist-pathogen transition in *Colletotrichum tofieldiae*. *Nature Communications* 14:5288

[2] Morcillo RJL, Singh SK, He D, An G, Vílchez JI, et al. 2020. Rhizobacterium-derived diacetyl modulates plant immunity in a phosphate-dependent manner. *The EMBO Journal* 39:EMBJ2019102602

[3] Bao DF, Tian XG, Samarakoon MC, Karunarathna SC, Luo ZL, et al. 2025. Biodiversity of lignicolous freshwater fungi from the Nanpan River Basin in Guizhou and Guangxi Provinces, China, with descriptions of fifteen species. *Mycosphere* 16(1):3695–3752

[4] Bao DF, Zhang JY, Lu YZ, Tian XG, Hyde KD, et al. 2025. Endophytic fungi associated with medicinal ferns in Guizhou Province, China Ⅰ: Morpho-molecular characterization of culturable endophytic fungi associated with *Dicranopteris spp*. *Mycosphere* 16(1):2259–2455

[5] Li QR, Habib K, Long SH, Wu YP, Zhang X, et al. 2024. Unveiling fungal diversity in China: new species and records within the Xylariaceae. *Mycosphere* 15(1):275–364

[6] Dissanayake LS, Samarakoon MC, Maharachchikumbura SSN, Hyde KD, Tang X, et al. 2024. Exploring the taxonomy and phylogeny of Sordariomycetes taxa emphasizing Xylariomycetidae in Southwestern China. *Mycosphere* 15(1):1675–1793

[7] Wang CG, Dai YC, Kout J, Gates GM, Liu HG, et al. 2024. Multi–gene phylogeny and taxonomy of *Physisporinus* (Polyporales, Basidiomycota). *Mycosphere* 15(1):1455–1521

[8] Lai Y, Cao X, Chen J, Wang L, Wei G, et al. 2020. Coordinated regulation of infection-related morphogenesis by the KMT2-Cre1-Hyd4 regulatory pathway to facilitate fungal infection. *Science Advances* 6(13):eaaz1659

[9] Miao Q, Wang Z, Yin Z, Liu X, Li R, et al. 2023. Nematode-induced trap formation regulated by the histone H3K4 methyltransferase AoSET1 in the nematode-trapping fungus *Arthrobotrys oligospora*. *Science China Life Sciences* 66(11):2663–2679

[10] Wei H, Zhong Z, Li Z, Zhang Y, Stukenbrock EH, et al. 2024. Loss of the accessory chromosome converts a pathogenic tree-root fungus into a mutualistic endophyte. *Plant Communications* 5(1):100672

[11] Han YK, Kim MD, Lee SH, Yun SH, Lee YW. 2007. A novel F-box protein involved in sexual development and pathogenesis in *Gibberella zeae*. *Molecular Microbiology* 63:768–779

[12] Zhou J, Wu S, Chen X, Liu C, Sheen J, et al. 2014. The *Pseudomonas syringae* effector HopF2 suppresses *Arabidopsis* immunity by targeting BAK1. *The Plant Journal* 77:235–245

[13] Banerjee M, Uppuluri P, Zhao XR, Carlisle PL, Vipulanandan G, et al. 2013. Expression of *UME6*, a key regulator of *Candida albicans* hyphal development, enhances biofilm formation via Hgc1-and Sun41-dependent mechanisms. *Eukaryotic Cell* 12:224–232

[14] He M, Xu Y, Chen J, Luo Y, Lv Y, et al. 2018. MoSnt2-dependent deacetylation of histone H3 mediates MoTor-dependent autophagy and plant infection by the rice blast fungus *Magnaporthe oryzae*. *Autophagy* 14(9):1543–1561

[15] Michielse CB, van Wijk R, Reijnen L, Manders EMM, Boas S, et al. 2009. The nuclear protein Sge1 of *Fusarium oxysporum* is required for parasitic growth. *PLoS Pathogens* 5(10):e1000637

[16] Li H, Wang D, Zhang DD, Geng Q, Li JJ, et al. 2022. A polyketide synthase from *Verticillium dahliae* modulates melanin biosynthesis and hyphal growth to promote virulence. *BMC Biology* 20(1):125

[17] Ujimatsu R, Takino J, Aoki S, Nakamura M, Haba H, et al. 2025. A fungal transcription factor converts a beneficial root endophyte into an anthracnose leaf pathogen. *Current Biology* 35(9):1989–2005.e6

[18] Zhou S, Li M, Wang P, Guo C, Zhang J, et al. 2025. A symbiotic filamentous gut fungus ameliorates MASH via a secondary metabolite–CerS6–ceramide axis. *Science* 388(6746):eadp5540

[19] Li Q, Duncan S, Li Y, Huang S, Luo M. 2024. Decoding plant specialized metabolism: new mechanistic insights. *Trends in Plant Science* 29:535–545

[20] Duc NH, van Doan C, Hamow KÁ, Le KH, et al. 2022. Volatile organic compounds shape belowground plant–fungi interactions. *Frontiers in Plant Science* 13:1046685

[21] Wang XJ, Wang Z, Han J, Su SH, Gong YX, et al. 2024. Sativene sesquiterpenoids from the plant endophytic fungus *Bipolaris victoriae* S27 and their potential as plant-growth regulators. *Journal of Agricultural and Food Chemistry* 72:2598–2611

[22] Manawasinghe IS, Hyde KD, Balasuriya A, Suwannarach N, Boonyuen N, et al. 2025. The emerging role of fungi in sustainable farming and global food security. *Mycosphere* 16(1):4936–5064

[23] López-González D, Costas-Gil A, Reigosa MJ, Araniti F, Sánchez-Moreiras AM. 2020. A natural indole alkaloid, norharmane, affects PIN expression patterns and compromises root growth in *Arabidopsis thaliana*. *Plant Physiology and Biochemistry* 151:378–390

[24] Vanneste S, Pei Y, Friml J. 2025. Mechanisms of auxin action in plant growth and development. *Nature Reviews Molecular Cell Biology* 26:648–666

[25] González Ortega-Villaizán A, King E, Patel MK, Pérez-Alonso MM, Scholz SS, et al. 2024. The endophytic fungus *Serendipita indica* affects auxin

distribution in *Arabidopsis thaliana* roots through alteration of auxin transport and conjugation to promote plant growth. *Plant, Cell & Environment* 47:3899−3919

[26] Djami-Tchatchou AT, Harrison GA, Harper CP, Wang R, Prigge MJ, et al. 2020. Dual role of auxin in regulating plant defense and bacterial virulence gene expression during *Pseudomonas syringae* PtoDC3000 pathogenesis. *Molecular Plant-Microbe Interactions* 33:1059−1071

[27] Han L, Zhou X, Zhao Y, Zhu S, Wu L, et al. 2020. Colonization of endophyte *Acremonium sp*. D212 in Panax notoginseng and rice mediated by auxin and jasmonic acid. *Journal of Integrative Plant Biology* 62:1433−1451

[28] Wang JK, Xiao Q, Zha XP, He ZJ, Kang JC. 2021. Endophyte *Fusarium lateritium* showing potato growth promotion and disease resistance and the construction of its genetic transformation system. *Mycosystema* 40:2008−2023 (in Chinese)

[29] Xiao Q, Li YJ, Wang JK, Zha XP, Huang JM, et al. 2022. Effects of an endophytic *Fusarium lateritium* on growth and disease resistance of tomato. *Journal of Huazhong Agricultural University* 41:173−180 (in Chinese)

[30] Zha XP, Li YJ, Wang JK, Xiao Q, Huang JM, et al. 2022. A strain of endophytic *Fusarium lateritium* promotes growth and resistance to bacterial wilt of tobacco. *Mycosystema* 41:1658−1671 (in Chinese)

[31] Huang J, He Z, Wang J, Zha X, Xiao Q, et al. 2023. A novel effector *FlSp1* inhibits the colonization of endophytic *Fusarium lateritium* and increases the resistance to *Ralstonia solanacearum* in tobacco. *Journal of Fungi* 9:519

[32] Dunken N, Widmer H, Balcke GU, Straube H, Langen G, et al. 2024. A nucleoside signal generated by a fungal endophyte regulates host cell death and promotes root colonization. *Cell Host & Microbe* 32:2161−2177.e7

[33] Maciá-Vicente JG, Jansson HB, Talbot NJ, Lopez-Llorca LV. 2009. Real-time PCR quantification and live-cell imaging of endophytic colonization of barley (*Hordeum vulgare*) roots by *Fusarium equiseti* and *Pochonia chlamydosporia*. *New Phytologist* 182:213−228

[34] Su ZZ, Mao LJ, Li N, Feng XX, Yuan ZL, et al. 2013. Evidence for biotrophic lifestyle and biocontrol potential of dark septate endophyte *Harpophora oryzae* to rice blast disease. *PLoS One* 8(4):e61332

[35] Hu K, Li R, Mo F, Ding Y, Zhou A, et al. 2023. Natural product osthole can significantly disrupt cell wall integrity and dynamic balance of *Fusarium oxysporum*. *Pesticide Biochemistry and Physiology* 196:105623

[36] Shi M, Li H, Guo W, Luo N, Chen J, et al. 2025. Tracking the infection dynamics of *Fusarium oxysporum* in *Codonopsis pilosula* based on GFP labelling. *Frontiers in Plant Science* 16:1586118

[37] Ma JC, Zhou Q, Zhou YH, Liao XG, Zhang YJ, et al. 2009. The size and ratio of homologous sequence to non-homologous sequence in gene disruption cassette influences the gene targeting efficiency in *Beauveria bassiana*. *Applied Microbiology and Biotechnology* 82:891−898

[38] Lahrmann U, Ding Y, Banhara A, Rath M, Hajirezaei MR, et al. 2013. Host-related metabolic cues affect colonization strategies of a root endophyte. *Proceedings of the National Academy of Sciences of the United States of America* 110:13965−13970

[39] Gross L. 2006. A chemical facilitator of plant-fungus communication. *PLoS Biology* 4:e241

[40] Han P, Wang C, Li F, Li M, Nie J, et al. 2024. *Valsa mali* PR1-like protein modulates an apple valine-glutamine protein to suppress JA signaling-mediated immunity. *Plant Physiology* 194:2755−2770

[41] Zhang XL, Gong XQ, Su XJ, Yu HX, Cheng SY, et al. 2023. The ubiquitin-binding protein MdRAD23D1 mediates drought response by regulating degradation of the proline-rich protein MdPRP6 in apple (*Malus domestica*). *Plant Biotechnology Journal* 21:1560−1576

[42] Luo L, Wu X, Fan J, Dong L, Wang M, et al. 2024. FBXO7 ubiquitinates PRMT1 to suppress serine synthesis and tumor growth in hepatocellular carcinoma. *Nature Communications* 15:4790

[43] Luo F, Tang G, Hong S, Gong T, Xin XF, et al. 2023. Promotion of *Arabidopsis* immune responses by a rhizosphere fungus via supply of pipecolic acid to plants and selective augment of phytoalexins. *Science China Life Sciences* 66:1119−1133

[44] Liu X, Liang D, Song W, Wang X, Duan W, et al. 2023. Tobacco roots increasing diameter and secondary lateral density in response to drought stress. *Plant Physiology and Biochemistry* 204:108122

[45] Ogata H, Goto S, Sato K, Fujibuchi W, Bono H, et al. 1999. KEGG: kyoto encyclopedia of genes and genomes. *Nucleic Acids Research* 27(1):29−34

[46] Zhu Z, Bani Ismail M, Shinohara M, Shinohara A. 2021. SCF^{Cdc4} ubiquitin ligase regulates synaptonemal complex formation during meiosis. *Life Science Alliance* 4:e202000933

[47] Miguel-Rojas C, Hera C. 2013. Proteomic identification of potential target proteins regulated by the SCF^{Fbp1}-mediated proteolysis pathway in *Fusarium oxysporum*. *Molecular Plant Pathology* 14:934−945

[48] Liu TB, Wang Y, Stukes S, Chen Q, Casadevall A, et al. 2011. The F-box protein Fbp1 regulates sexual reproduction and virulence in *Cryptococcus neoformans*. *Eukaryotic Cell* 10:791−802

[49] Redkar A, Gimenez Ibanez S, Sabale M, Zechmann B, Solano R, et al. 2022. *Marchantia polymorpha* model reveals conserved infection mechanisms in the vascular wilt fungal pathogen *Fusarium oxysporum*. *New Phytologist* 234:227−241

[50] Xiao Y, Sun G, Yu Q, Gao T, Zhu Q, et al. 2024. A plant mechanism of hijacking pathogen virulence factors to trigger innate immunity. *Science* 383:732−739

[51] Zhao B, He D, Gao S, Zhang Y, Wang L. 2022. Hypothetical protein FoDbp40 influences the growth and virulence of *Fusarium oxysporum* by regulating the expression of isocitrate lyase. *Frontiers in Microbiology* 13:1050637

[52] Long Y, Chen X, Chen J, Zhang H, Lin Y, et al. 2025. Golgi-associated retrograde protein (GARP) complex recruits retromer to *trans*-Golgi network for FgKex2 and FgSnc1 recycling, necessary for the development and pathogenicity of *Fusarium graminearu*m. *New Phytologist* 246:666−688

[53] Chen D, Shu D, Wei Z, Luo D, Yang J, et al. 2023. Combined transcriptome and proteome analysis of Bcfrp1 involved in regulating the biosynthesis of abscisic acid and growth in *Botrytis cinerea* TB-31. *Frontiers in Microbiology* 13:1085000

[54] Adamek M, Kavčič A, Debeljak M, Šala M, Grdadolnik J, et al. 2024. Toxicity of nitrophenolic pollutant 4-nitroguaiacol to terrestrial plants and comparison with its non-nitro analogue guaiacol (2-methoxyphenol). *Scientific Reports* 14:2198

[55] Ma H, Li J, Luo A, Lv H, Ren Z, et al. 2023. Vanillin, a newly discovered autotoxic substance in long-term potato continuous cropping soil, inhibits plant growth by decreasing the root auxin content and reducing adventitious root numbers. *Journal of Agricultural and Food Chemistry* 71(45):16993−17004

[56] Roy A, Tamuli R. 2022. Heat shock proteins and the calcineurin-crz1 signaling regulate stress responses in fungi. *Archives of Microbiology* 204:240

[57] Sheng X, Himo F. 2020. Computational study of pictet–spenglerase strictosidine synthase: reaction mechanism and origins of enantioselectivity of natural and non-natural substrates. *ACS Catalysis* 10:13630−13640

[58] Maresh JJ, Giddings LA, Friedrich A, Loris EA, Panjikar S, et al. 2008. Strictosidine synthase: mechanism of a pictet–spengler catalyzing enzyme. *Journal of the American Chemical Society* 130:710−723

[59] Aoun N, Tauleigne L, Lonjon F, Deslandes L, Vailleau F, et al. 2017. Quantitative disease resistance under elevated temperature: genetic basis of new resistance mechanisms to *Ralstonia solanacearum*. *Frontiers in Plant Science* 8:1387

[60] Hao MJ, Chen PN, Li HJ, Wu F, Zhang GY, et al. 2022. β-carboline alkaloids from the deep-sea fungus *Trichoderma* sp. MCCC 3A01244 as a new type of anti-pulmonary fibrosis agent that inhibits TGF-β/smad signaling pathway. *Frontiers in Microbiology* 13:947226

[61] Gao M, Wang X, Wang D, Xu F, Ding X, et al. 2009. Regulation of cell death and innate immunity by two receptor-like kinases in *Arabidopsis*. *Cell Host & Microbe* 6:34−44

[62] Frigerio M, Alabadí D, Pérez-Gómez J, García-Cárcel L, Phillips AL, et al. 2006. Transcriptional regulation of gibberellin metabolism genes by auxin signaling in *Arabidopsis*. *Plant Physiology* 142:553−563

[63] Mäkilä R, Wybouw B, Smetana O, Vainio L, Solé-Gil A, et al. 2023. Gibberellins promote polar auxin transport to regulate stem cell fate decisions in cambium. *Nature Plants* 9:631−644

[64] Cao C, Xue C. 2021. More than just cleaning: ubiquitin-mediated proteolysis in fungal pathogenesis. *Frontiers in Cellular and Infection Microbiology* 11:774613
[65] Berthiller F, Lemmens M, Werner U, Krska R, Hauser MT, et al. 2007. Short review: metabolism of the *Fusarium mycotoxins* deoxynivalenol and zearalenone in plants. *Mycotoxin Research* 23:68–72
[66] Wu L, Bian W, Abubakar YS, Lin J, Yan H, et al. 2024. FvKex2 is required for development, virulence, and mycotoxin production in *Fusarium verticillioides*. *Applied Microbiology and Biotechnology* 108:228
[67] Schmatz DM, Abruzzo G, Powles MA, Mcfadden DC, Balkovec JM, et al. 1992. Pneumocandins from *Zalerion arboricola* IV. Biological evaluation of natural and semisynthetic pneumocandins for activity against *Pneumocystis carinii* and *Candida* species. *The Journal of Antibiotics* 45:1886–1891
[68] Liu X, Huang Y, Chen W, Jiang D, Cheng J. 2025. Functions and mechanisms of secreted proteinaceous effectors of broad-host-range necrotrophic fungal pathogens. *Annual Review of Phytopathology* 63:89–115
[69] Shi J, Wang H, Li M, Mi L, Gao Y, et al. 2024. *Alternaria* TeA toxin activates a chloroplast retrograde signaling pathway to facilitate JA-dependent pathogenicity. *Plant Communications* 5(3):100775